UNITED NATIONS EDUCATIONAL, SCIENTIFIC AND CULTURAL ORGANIZATION
INTERNATIONAL CENTRE FOR THEORETICAL PHYSICS
I.C.T.P., P.O. BOX 586, 34100 TRIESTE, ITALY, CABLE: CENTRATOM TRIESTE

H4.SMR/782-19

Second Workshop on
Three-Dimensional Modelling of Seismic Waves
Generation, Propagation and their Inversion

7 - 18 November 1994

Seismic Source Studies for Point-like Sources

P. Suhadolc

Istituto di Geodesia e Geofisica
Università di Trieste
Trieste, Italy

Geophys. J. Int. (1994) **116**, 784–798

Linearized waveform inversion of local and near-regional events for source mechanism and rupturing processes

W. J. Mao,[1,2] G. F. Panza[1,3] and P. Suhadolc[1]

[1] *Istituto di Geodesia e Geofisica, Università di Trieste, Via dell'Università 7, 34100 Trieste, Italy*
[2] *Department of Earth Sciences, University of Leeds, Leeds* LS2 9JT, *UK*
[3] *International Center for Theoretical Physics, 34100 Trieste, Italy*

Accepted 1993 August 25. Received 1993 August 24; in original form 1992 May 27

SUMMARY

We have developed an algorithm which can, given an initial trial solution, determine simultaneously earthquake-source mechanism, hypocentre and source-time function from the inversion of broad-band waveform data of local and near-regional events (epicentral distances less than 10°).

The forward modelling of the seismic ground motion is computed for frequencies up to 10 Hz by multimodal summation in layered anelastic media. The non-linear damped least-squares technique is used to minimize the difference between the theoretical and the observed seismograms in the time domain. The use of a weighting matrix and variable damping factor in each iteration avoids the problem of the ill-conditioned matrix inverse and guarantees the stability of the inverse solution. To reduce the influence of the earth model error on the inversion, for each source–receiver path the most appropriate layered earth model can be used.

The algorithm has been tested against synthetic data to investigate the inversion convergence and the dependence of the solution on the fact that the assumed earth model is never equal to the true one. The synthetic tests indicate that if the earth model(s) is (are) adequate, the inversion converges rapidly to the 'true' solution. The sensitivity of the method to the starting model is found to be frequency dependent. The initial location can be in error by approximately the *P*- or *S*-wave wavelength and the initial source mechanism parameters can differ considerably from 'true' model. The focal depth and source-time function depend strongly on the crustal model.

Subsequently, the algorithm has been successfully applied to two events: a near-regional and a local event. The first is the 1974 March 22 event which occured in Albania, was recorded at Bari and Trieste LP stations (like WWSSN), and has been analysed using two differnt structural models based upon surface-wave dispersion measurements. The second is the Friuli event of 1987 December 27, which was recorded at five digital SP local stations, and has been analysed using a local crustal model obtained from the inversion of *P*- and *S*-wave arrival times.

Key words: local regional events, near-regional events, source parameters, waveform inversion.

1 INTRODUCTION

In the past decade, many methods dealing with the problem of seismic-waveform inversion for the source mechanism have been developed. Their main advantage, in comparison with the classical body-wave polarity studies, is that complete seismograms are used in the analysis. This allows the retrieval not only of the fault-plane solution and hypocentral location, but also of the source-time history.

Stump & Johnson (1977) addressed the general problem of the determination of moment tensor and source-time function using seismic-waveform data. For a point source the problem can be shown to be linear in both the time and frequency domains. The first attempt to determine the seismic-moment tensor and the relative source-time function at the source centroid by waveform fitting of body waves was made by Langston (1981). However, this linear approach needs an *a priori* assumption about the true

hypocentral location, which may not be known precisely enough. In order to overcome this difficulty, Dziewonski, Chou & Woodhouse (1981) proposed a new approach. They expanded, to the first order, the point-source response with respect to small perturbations in the source coordinates and origin time. In this case, the non-linear inversion for the hypocentre location is reduced to a linearized inversion, and the hypocentre location and seismic moment tensor at the source centroid can be determined simultaneously. Their approach is applicable to long-period, far-field earthquake data. A similar approach was developed for teleseismic events by Nabelek (1984), who extended the method to short-period body-wave data.

New networks of broad-band seismic stations are currently being deployed for studying local and near-regional (for epicentral distances smaller than 10°) earthquakes. It is important to determine how many of the source parameters can be obtained from full waveform analysis of the new local and regional broader band data, and whether the obtained source parameters are of higher quality than those determined routinely by the usual high-gain seismic networks. The previous methods seem not to be able to give a satisfactory answer, since they are only applicable to long-period, teleseismic events. Recently, Ritsema & Lay (1992) have shown that application of a long-period regional CMT procedure to three-component data recorded in the western US is an effective way to obtain moment tensor information in near real-time. Attempts to retrieve source parameters from regional and local broad-band waveforms have been made by Dreger & Helmberger (1991, 1992), Fan & Wallace (1991), Walter (1992) and Sileny, Panza & Campus (1992). These algorithms still need *a priori* assumption about the true epicentre location, and the inversion is done at various focal depths. Except Sileny *et al.*'s algorithm, high-frequency ($f > 2$) data were not used in the inversion. In this paper, we present a joint local–regional CMT and source-time function inversion method which is applicable to high-frequency data ($f_{max} = 10$ Hz). Our algorithm has the following characteristics: (1) high-frequency data from broad-band seismic stations and accelerometers can be used, this being an extension of the Harvard CMT approach (Dziewonski *et al.* 1981) to near-regional events with surface waves included; (2) strike, dip, rake, hypocentre and source-time function are simultaneously determined by assuming as a system of forces equivalent to a dislocation, the double-couple with zero moment, this last assumption restricting us to a model that is a quite appropriate for most earthquakes; (3) for each source–receiver path a different (most appropriate) layered earth model can be used, thus reducing the influence of the earth-model error on the solution of the inverse problem.

The forward modelling of earthquake ground motion is made using the multimodal summation method in layered anelastic media for frequencies up to 10 Hz (Panza 1985; Panza, Suhadolc & Chiaruttini 1986; Panza & Suhadolc 1987). The algorithm can be extended to laterally heterogeneous anelastic media following the results of Vaccari *et al.* (1989). The non-linear least-squares technique is used to minimize the difference between the theoretical and the observed seismograms in the time domain. The partial derivatives of the theoretical seismogram with respect to the model parameters can be calculated analytically. In order to avoid the instability of the inverse matrix due to the small eigenvalues, the generalized inverse theory with a damping factor is used.

Using synthetic data we tested the procedure against point-source models. Then we applied it to the 1974 March 22 event which occurred in Albania, and which was recorded at the Bari and Trieste LP stations (like WWSSN), and to the Friuli event of 1987 December 27, which was recorded at five digital SP local stations.

The purpose of this paper is to develop a methodology which is proved to work both for regional and local events. It can be used to compare the source-time functions of a set of small events recorded by a local network.

2 FORMULATION OF THE WAVEFORM INVERSION

The ground motion due to an earthquake is determined by the earthquake source properties and the Earth structure. If the Earth structure is known, the earthquake source parameters (strike, dip, rake, depth, epicentre and source-time function) can be obtained by minimizing the difference between the observed seismograms and the theoretical ones. This is because seismic phases provide us with information on source location while amplitudes of seismic waves are related to the source radiation pattern (mechanism).

If the epicentral distance and the minimum wavelength in the signal are much larger than the source dimension, the earthquake source can be considered as a point source. In such a case the dislocation at the source can be schematized by a double couple with zero moment (Burridge & Knopoff 1964), whose orientation depends on the geometry of the fault plane and whose location depends on the hypocentral coordinates. The time dependence of the source can be described by the rate of seismic moment release, i.e. the source-time function.

Even if in this formulation the orders of space and time source moments are different, such a parametrization is acceptable when applied to point-source-like events. In fact, for such 'small' events the internal space structure of the source is more difficult to resolve than the energy release of the source in time. Of course, in such a formulation the possible spatial peculiarities of the rupturing process are transformed into complexities of the source-time function. The case of a spatially extended source will be treated in a future paper.

The ground motion excited by a point source with a source-time function $\dot{m}(t)$, $m(t)$ being the scalar moment release in time, and recorded by an instrument with response function $i(t)$, may be expressed as

$$s(t) = i(t) * u(t) * \dot{m}(t), \tag{1}$$

where the asterisk denotes the convolution operator and $u(t)$ is the Rayleigh- or Love-modes dispalcement at the free surface due to a point source with a time dependence given by a Heaviside function. The instrumental response function will be omitted in the following equations. The multimodal summation for the computation of broad-band synthetic seismogram, with a maximum frequency of 10 Hz, has been discussed in full detail by Panza (1985), Panza & Suhadolc (1987) and Florsch *et al.* (1991). Here we give only some

equations that are related to the source parameters. For a double-couple with zero moment, following Panza, Schwab & Knopoff (1973), the Rayleigh-mode displacement can be written as

$$u_r(t) = FT^{-1}\left(\sum_j U_{rj}\right) = FT^{-1}\sum_j \mathbf{R}(\omega)\,|\mathbf{n}|\,k^{1/2} \times \exp\left(\frac{-i3\pi}{4}\right)\chi(\xi,\eta,\lambda,h)E\varepsilon_0\frac{\exp(-ik\Delta)}{\sqrt{2\pi\Delta}}, \quad (2)$$

$$u_z(t) = FT^{-1}\sum_j\left[\varepsilon_0\exp\left(\frac{-i\pi}{2}\right)\right]^{-1}U_{rj}, \quad (3)$$

$$u_\theta(t) = 0, \quad (4)$$

where $\mathbf{R}(\omega)$ is the Fourier transform of the equivalent point-force time function, $\mathbf{n}$ is the unit vector perpendicular to the fault and has units of length, k is the wavenumber, E^{-1} is the product of phase velocity, group velocity and energy integral, I_1, χ is the radiation pattern defined in the Appendix, Δ is the epicentral distance. FT^{-1} is the inverse Fourier transform operator. The energy integral is defined as

$$I_1 = \int_0^\infty \rho\left\{\left[\frac{w(z)}{w(0)}\right]^2 + \left[\frac{u(z)}{w(0)}\right]^2\right\}dz, \quad (5)$$

where ρ is the density; $u(z)$ and $w(z)$ are the horizontal and vertical components of Rayleigh-mode particle motion at depth z; $\varepsilon_0 = u(0)/w(0)$. The six source parameters ξ, η, λ, h, x and y are the strike–receiver angle, the dip angle of the fault, the rake angle, the focal depth and the epicentral coordinates, respectively.

The unknown source-time function, $\dot{m}(t)$, is parametrized with a series of triangular elements with different weights. The width of each element is specified to be δt, and the time shift between two subsequent elements to be $\delta\tau$. Thus

$$\dot{m}(t) = \sum_{j=1}^{K} w_j g[t - (j-1)\,\delta\tau], \quad (6)$$

where

$$g(t) = \begin{cases} \dfrac{2}{\delta t}\left[1 - \left|\dfrac{2t}{\delta t} - 1\right|\right] & 0 < t < \delta t \\ 0 & \text{elsewhere} \end{cases}$$

is a triangular element with unit area, i.e. unit seismic moment. δt is determined by considering the bandwidth of the data, $\delta\tau$ is specified to be smaller or equal to $\frac{\delta t}{2}$. For a set of given δt and $\delta\tau$, the time function duration and shape are controlled by the number of triangular elements, K, and their weights w_j. We impose the no-backward slip constraint on the fault, so the weights w_j at each iteration are set equal to zero when they become negative.

The Fourier time transform, $M(\omega)$, of the source-time function $\dot{m}(t)$ can be written as

$$M(\omega) = G(\omega)\sum_{j=1}^{K} w_j \exp[-i\omega(j-1)\,\delta\tau], \quad (7)$$

where

$$G(\omega) = \frac{\sin^2\left(\dfrac{\omega\,\delta t}{4}\right)}{\left(\dfrac{\omega\,\delta t}{4}\right)^2}\exp\left(\frac{-i\omega\,\delta t}{2}\right), \quad (8)$$

is the Fourier transform of $g(t)$.

Since the theoretical seismogram is a non-linear function of the source parameters we perform the minimization by a linearized inversion technique. The standard linearized equation is given by

$$\mathbf{A}\,\delta\mathbf{x} = \mathbf{r}, \quad (9)$$

where $\mathbf{A}$ is the Jacobian matrix of partial derivatives of the theoretical seismograms with respect to source parameters, $\delta\mathbf{x}$ is the unknown vector of N source parameter perturbations, and $\mathbf{r}$ is the vector containing the differences $o_j - s_j$ $(j = 1, 2, \ldots, M)$ between the observed and the theoretical seismograms. The structure of matrix $\mathbf{A}$ is given by

$$\begin{bmatrix}
\frac{\partial s_1(t_1)}{\partial\xi} & \frac{\partial s_1(t_1)}{\partial\eta} & \frac{\partial s_1(t_1)}{\partial\lambda} & \frac{\partial s_1(t_1)}{\partial h} & \frac{\partial s_1(t_1)}{\partial x} & \frac{\partial s_1(t_1)}{\partial y} & \frac{\partial s_1(t_1)}{\partial w_1} & \cdots & \frac{\partial s_1(t_1)}{\partial w_K} \\
\vdots & \vdots & \vdots & \vdots & \vdots & \vdots & \vdots & \cdots & \vdots \\
\frac{\partial s_1(t_{m1})}{\partial\xi} & \frac{\partial s_1(t_{m1})}{\partial\eta} & \frac{\partial s_1(t_{m1})}{\partial\lambda} & \frac{\partial s_1(t_{m1})}{\partial h} & \frac{\partial s_1(t_{m1})}{\partial x} & \frac{\partial s_1(t_{m1})}{\partial y} & \frac{\partial s_1(t_{m1})}{\partial w_1} & \cdots & \frac{\partial s_1(t_{m1})}{\partial w_K} \\
\cdots & \cdots & \cdots & \cdots & \cdots & \cdots & \cdots & \cdots & \cdots \\
\frac{\partial s_n(t_1)}{\partial\xi} & \frac{\partial s_n(t_1)}{\partial\eta} & \frac{\partial s_n(t_1)}{\partial\lambda} & \frac{\partial s_n(t_1)}{\partial h} & \frac{\partial s_n(t_1)}{\partial x} & \frac{\partial s_n(t_1)}{\partial y} & \frac{\partial s_n(t_1)}{\partial w_1} & \cdots & \frac{\partial s_n(t_1)}{\partial w_K} \\
\vdots & \vdots & \vdots & \vdots & \vdots & \vdots & \vdots & \cdots & \vdots \\
\frac{\partial s_n(t_{mn})}{\partial\xi} & \frac{\partial s_n(t_{mn})}{\partial\eta} & \frac{\partial s_n(t_{mn})}{\partial\lambda} & \frac{\partial s_n(t_{mn})}{\partial h} & \frac{\partial s_n(t_{mn})}{\partial x} & \frac{\partial s_n(t_{mn})}{\partial y} & \frac{\partial s_n(t_{mn})}{\partial w_1} & \cdots & \frac{\partial s_n(t_{mn})}{\partial w_K}
\end{bmatrix}$$

where s_i and t_{mi} are, respectively, the seismogram and the length of the time window used in the inversion of the record at the ith station, t_1 the starting time of the window, $M = \sum_{i=1}^{n} mi$.

Since the amplitudes of the different station records are, in general, quite different due to differences in the epicentral distances and azimuths, we must normalize these seismic signals in order that all the signals contribute equally in the linearized equation. However, the amplitude variation with azimuth provides us with information on the source radiation pattern. To keep the information on the

source radiation pattern in the inversion, the r_j are normalized as follows:

$$r_j = \left[\frac{o_i(t_j)}{o^{\max}} - \frac{s_i(t_j)}{s^{\max}}\right]\left(\frac{o^{\max}}{o_i^{\max}}\right), \tag{10}$$

where $o_i^{\max}$ is the absolute value of the maximum amplitude of the observed signal at the ith station and $o^{\max}$ and $s^{\max}$ are, respectively, the maximum absolute value of the observed and theoretical amplitude of all stations. Because of the normalization, the corresponding modification should also be applied to the matrix **A**, resulting in an amplitude constraint being added to the inversion equations.

In order to solve eq. (9), the inverse of the Jacobian matrix **A** should be found. **A** can be factored using the singular-value decomposition (SVD):

$$\mathbf{A} = \mathbf{U}\mathbf{\Lambda}\mathbf{V}^{\mathrm{T}}, \tag{11}$$

where **U** is an $M \times M$ orthogonal matrix, **V** is an $N \times N$ orthogonal matrix, **Λ**, is a P-diagonal matrix formed by the singular values λ_i ($i = 1, 2, \ldots, N$) of the matrix **A**. The λ_i are the non-negative square roots of the eigenvalues of $\mathbf{A}^{\mathrm{T}}\mathbf{A}$, and $P = \min(M, N)$. For overdetermined systems, $P = N$. According to the properties of an orthogonal matrix, the inverse of the matrix **A** is

$$\mathbf{A}^{+} = \mathbf{V}\mathbf{\Lambda}^{-1}\mathbf{U}^{\mathrm{T}}, \tag{12}$$

where $\mathbf{\Lambda}^{-1}$ is defined by $\lambda_i^{-1} = \dfrac{1}{\lambda_i}$ for $\lambda_i > 0$, and $\lambda_i^{-1} = 0$ for $\lambda_i = 0$. This means that the inverse of eq. (12) always exists, even when the matrix is singular, but it will not give us a unique solution because of the existence of zero eigenvalues (Carrion 1989). In addition, very small eigenvalues make some components of the solution vector unstable. In order to avoid these problems, it is convenient to introduce the so-called damping parameter θ^2 (Aki & Richards 1980) and to write

$$\delta\mathbf{x} = \mathbf{V}(\mathbf{\Lambda}^2 + \theta^2\mathbf{I})^{-1}\mathbf{\Lambda}\mathbf{U}^{\mathrm{T}}\mathbf{r}. \tag{13}$$

The damping parameter, which is not determined *a priori* and is usually found by trial and error, eliminates the influence of zero and very small eigenvalues. Its choice is crucial in the convergence rate and stability of the solution. We allow θ^2 to be variable, its value depending on the ratio of the largest to the smallest singular value in each iteration.

Equation (9) is quasi-linear since **A** changes in response to the current solution vector **x** and the minimum is reached by an iterative procedure.

Since the parameter of focal mechanism, source location and source-time function have different physical dimensions, there are large differences among the elements of the matrix **A**. In order to avoid the instability due to an ill-conditioned inverse matrix, we have weighted the partial derivative matrix **A** and the perturbation to the model vector $\delta\mathbf{x}$ in eq. (9) with a diagonal weighting matrix

$$\mathbf{A}\mathbf{W}\,\delta\mathbf{x}' = \mathbf{r}, \tag{14}$$

where $\delta\mathbf{x}' = \mathbf{W}^{-1}\,\delta\mathbf{x}$. The elements of the weighting matrix, **W**, can be conveniently chosen in the following way. We find the maximum value in each column of the matrix **A**, $\max[A_{ij}]$ for $j = 1, 2, \ldots, N$, and then the minimum value among all the $\max[A_{ij}]$, i.e.

$$W_{\min} = \min\{\max[A_{i1}], \max[A_{i2}], \ldots, \max[A_{iN}]\}. \tag{15}$$

Then the values

$$W_{jj} = \frac{W_{\min}}{\max[A_{ij}]} \qquad (j = 1, 2, \ldots, N) \tag{16}$$

are taken as the diagonal elements of the weighting matrix **W**. The use of the weighting matrix and of the variable damping factor guarantees the stability and fast convergence rate of the inversion.

For a double-couple point source the six unknown source parameters ξ, η, λ, h, x and y plus the source-time function must be determined. The partial derivatives of the synthetic seismogram, $s(t)$, with respect to the source parameters can be calculated analytically using eq. (2) in the frequency domain. The partial derivative of $s(t)$ with respect to the epicentral coordinates can be easily derived by using chain rule

$$\frac{\partial s}{\partial x} = \frac{\partial s}{\partial \Delta}\frac{\partial \Delta}{\partial x}, \qquad \frac{\partial s}{\partial y} = \frac{\partial s}{\partial \Delta}\frac{\partial \Delta}{\partial y}, \tag{17}$$

where

$$\frac{\partial s(t)}{\partial \Delta} = -FT^{-1}\left\{\left[ik + \frac{1}{2\Delta}\right]U(\omega)M(\omega)\right\}, \tag{18}$$

where $U(\omega)$ and $M(\omega)$ are the Fourier transforms of $u(t)$ and $\dot{m}(t)$, respectively, and ω is the angular frequency. $\dfrac{\partial s}{\partial \xi}$, $\dfrac{\partial s}{\partial \eta}$ and $\dfrac{\partial s}{\partial \lambda}$ are related to the complex radiation pattern function which consists of some sine and cosine functions of ξ, η and λ. The computation of $\dfrac{\partial s}{\partial h}$ requires the calculation of the partial derivatives of the eigenfunctions with respect to the depth, which can be expressed as a linear combination of the eigenvalues at the depth h (Harkrider 1970). For details on these computations see the Appendix. The partial derivative $\dfrac{\partial s(t)}{\partial w_j}$ is easily obtained from eq. (6).

In order to test the results of the analytical calculation, the partial derivatives are also calculated numerically

$$\frac{\partial s(t)}{\partial x_i} = \frac{s[(1+\varepsilon)x_i] - s[(1-\varepsilon)x_i]}{2\varepsilon x_i}, \tag{19}$$

where ε is a small quantity, its typical value ranging between 10^{-4} to 10^{-5}, and x_i ($i = 1, \ldots, 5$) indicates ξ, η, λ, h, Δ in the order. Fig. 1 shows the partial derivatives obtained from the analytical and the numerical method. The little differences among the time series are well within the errors of the numerical method.

A relevant optimization of the inversion code is obtained by performing the computations of the partial derivatives with respect to the source parameter in the frequency domain. Furthermore, the computation of the partial derivatives does not require the solution of a new eigenvalue problem, therefore the use of an iterative inversion scheme is possible.

For a given earthquake, the complete seismogram at a given station equipped with a vertical-component instrument contains the following relevant information about the source

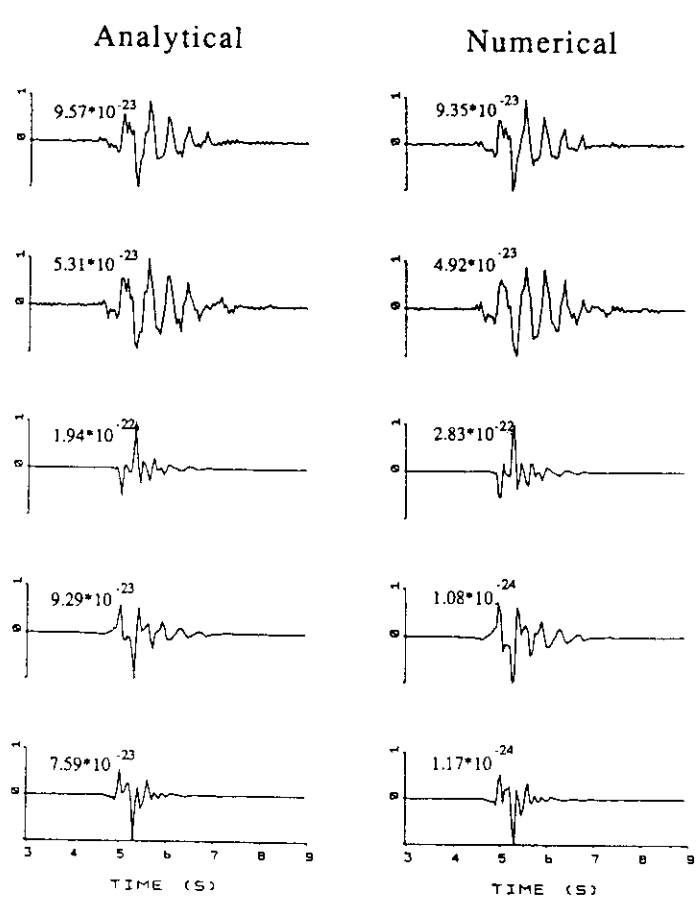

Figure 1. Comparison between the results of the analytical and numerical computation of partial derivatives. Starting from above, the derivatives of the theoretical seismogram with respect to epicentral distance, Δ, depth, h,rake, λ, dip, η, and strike, ξ, are shown.

(location and mechanism): P, S and P–SV amplitudes and phases. Only four of these six quantities are linearly independent. Other complexities in the waveforms, like reflected and converted waves, dispersed surface waves, etc., are due to the heterogeneity of the Earth. This can be easily seen from the displacement response to a point force within a homogeneous elastic half-space medium (Aki & Richards 1980, Section 4.2). Although the secondary waves depend on geometrical source parameters they are related to the P and S waves, and thus do not provide any futher independent information. For a double-couple source, in addition to the spatial (hypocentral) coordinates, there are three independent-source geometrical parameters to be determined; strike, dip and rake. Therefore, to determine the source geometry, the vertical-component records at two stations are sufficient. Thus, in this paper, we will limit our analysis to vertical-component records, since the use of the horizontal-component records is not strictly necessary and many networks are equipped with vertical-component instruments. The full inversion of three-component records will be treated in a future paper.

Once we have obtained the source parameters and the source-time function, we determine the point-source scalar seismic moment with the following expression:

$$M_0 = \frac{1}{n}\sum_{i=1}^{n}\frac{O_i^{\max}}{S_i^{\max}}\int_0^{t_k}\dot{m}(t)\,dt, \tag{20}$$

where $O_i^{\max}$ and $S_i^{\max}$ are the maxima of the envelopes of the observed and theoretical seismograms at ith station, respectively, while the value of the integral represents the area below the curve $\dot{m}(t)$, which is equal to the scalar seismic moment of the theoretical seismograms; and t_k is given by

$$t_k = \delta t + (K-1)\,\delta\tau. \tag{21}$$

The discrepancies of the scalar seismic moment as determined from different stations are actually small, since we included the amplitude constraint in the inversion equations.

3 TEST WITH SYNTHETIC DATA IN THE POINT-SOURCE APPROXIMATION

In this section, we apply our formulation of the linearized inversion theory to synthetic data in order to prove the ability of the method to retrieve simultaneously source mechanism, location and time function. Three examples are given. The first two show the convergence of the inversion procedure to different frequency contents, assuming a given earth model, while the third gives some insight as to how much the outcome of the inversion depends on the fact that the assumed earth model is never equal to the true one. The procedure runs as follows: some seismograms are calculated

for a set of model parameters (focal depth, epicentral location, source mechanism and time function) and for an assumed earth model. These seismograms are considered to be the observed signals, and the model parameters used in the computation are the 'true' model. The initial model is, of course, chosen to be different to the 'true' model; starting from the initial model, we iterate until a minimum residual (rms error between the synthetic and observed waveforms) is reached.

3.1 Regional event with a maximum frequency of 1 Hz

We assume that an earthquake is recorded by the vertical-component instruments of three different stations. The focal depth and the source mechanism of the 'true' model at the source centroid are $h = 15$ km, $\xi = 278°$, $\eta = 39°$, $\lambda = 174°$. The location of the stations and of the epicentre, the source-time function and the pertinent time series (displacement) are shown in Fig. 2 (with label B). The

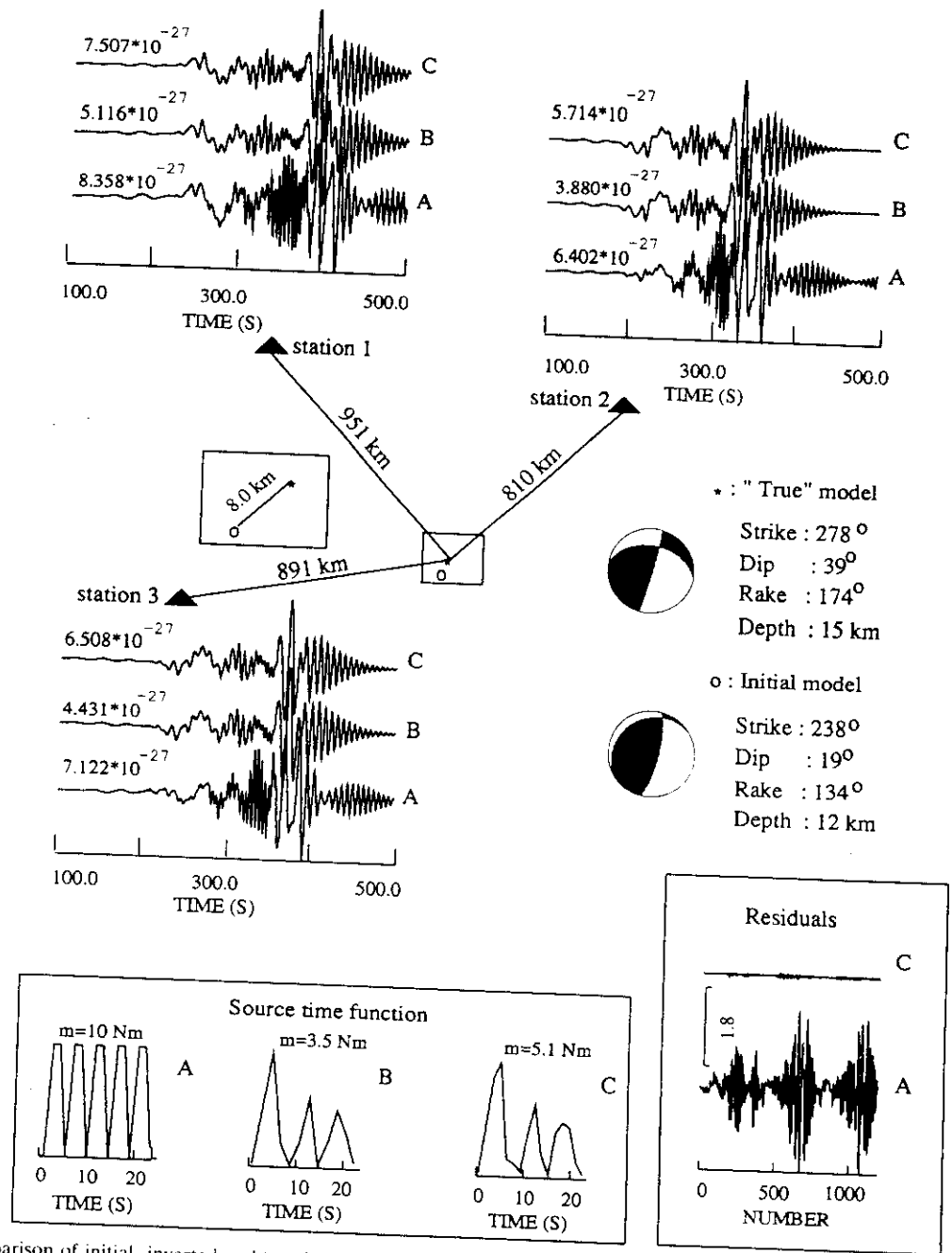

Figure 2. Comparison of initial, inverted and 'true' waveforms; source parameters and stations used in the synthetic test; and residuals of the initial and inverted seismograms with respect to the 'true' ones. The number on the left-hand side of each seismogram represents the maximum amplitude (in m). In this and the following figures the labels A, B and C denote, in order, the initial, the 'true' and the inverted model. The asterisk represents the 'true' epicentre, while the open circle indicates the initial epicentre used in the inversion. The inverted mechanism and hypocentre are same as the 'true' ones.

Table 1. Crustal and upper mantle structural model SADRIA1, $Q_p = 2.5A_v$.

Thickness (km)	Density (g/cm^3)	P-wave velocity (km/s)	S-wave velocity (km/s)	Q_s
1.0	1.03	1.52	0.00	0.00
4.0	2.40	3.98	2.30	100
10.0	2.70	5.54	3.20	200
6.0	2.80	6.06	3.50	200
6.0	2.75	5.89	3.40	100
10.0	3.00	6.58	3.80	200
45.0	3.30	7.80	4.50	400
90.0	3.30	8.00	4.60	400

source-time function of the 'true' model consists of three bursts of moment release (total moment 3.5 Nm) which is parametrized by 10 triangular elements with a rise time of 4.0 s, a time delay of 2.0 s and weights being 0.5, 1.0, 0.2, 0.0, 0.2, 0.6, 0.0, 0.2, 0.5 and 0.3, respectively. The maximum frequency of the seismograms is 1 Hz. The earth model with one water layer overlying a series of solid layers, on top of which the receivers are placed, is shown in Table 1.

The real problem in a non-linear inversion is the convergence to local minima. We investigate this problem with the following test. We want to know how far the initial model can be from the true model and still have this method converge to the 'true' model. The initial model is started with a blind guess ($h = 10$ km, $\xi = 180°$, $\eta = 10°$, $\lambda = 90°$, epicentre deviation 20 km). Following a Monte Carlo process with sampling interval 1 km, 20°, 5°, 20° and 3 km, respectively, we found that in this test the maximum allowed deviations of the initial model from the 'true' model are about $\delta\xi = 40°$, $\delta\eta = 20°$, $\delta\lambda = 40°$, $\delta h = 3$ km, $\delta\Delta = 8$ km, the time function being arbitrary under the condition of a rise time δt small enough, its typical value is between two and eight times that of the sampling interval of the seismogram used in the inversion. If the deviation is beyond these boundary values the inversion process diverges. We demonstrate this with an example. The initial source parameter model is chosen as $h = 12$ km, $\xi = 238°$, $\eta = 19°$, $\lambda = 134°$. The initial epicentre is 8.0 km away from the 'true' epicentre, and the initial time function is formed by $K = 15$ triangular elements each with a rise time of 3.0 s and a time delay of 1.5 s, the weights being 1.0, 1.0, 0.0, 1.0, 1.0, 0.0, . . . , 1.0, 1.0, 0.0, respectively (see Fig. 2 with label A). After seven iterations the solution converges to the 'true' model. The results are shown in Fig. 2. The seismograms and source-time functions are normalized by their maximum amplitudes. The labels A, B and C in Fig. 2. are associated with the initial, 'true' and inverted source parameters, respectively. The differences in the maximum amplitudes of the inverted seismograms with respect to the 'true' ones are due to the different scalar seismic moments. The seismic moment obtained from eq. (20) is equal to 3.47 Nm, which matches closely the 'true' one, which is 3.5 Nm. Although we use in the iterative procedure, a rise time and time delay that are different from the 'true' model, the inversion still converges rapidly. This indicates that as long as we choose, for each $\dot{m}(t)$, a rise time small enough compared with the total rupture process, the time function can be correctly retrieved. In order to illustrate the inversion convergence, we give the results of each iteration in Fig. 3, where only the seismograms at station 2 are shown. We did not include random noise in the test, since waveform inversion is little affected by random errors, as long as they are smaller than 20 per cent of the signal's maximum amplitude. This has been theoretically proved by Mao & Gubbins (1993) and discussed by Sileny *et al.* (1992) using synthetic noisy data. The damping factor θ^2 is chosen as 1.0 per cent of the largest singular value in each iteration.

If the station distribution is appropriate and the structural parameters are sufficiently well known, the seismic-source parameters can, in principle, be determined very easily; for instance, the time function could be found with the deconvolution method. However, deconvolution is usually unstable in most applications, and no generally useful computational technique is available (e.g. Ruff & Kanamori 1983). This shortcoming can be bypassed easily using the linear inversion scheme described in Section 2. If we assume the source-time function to be the only unknown, we obtain the correct solution after just three interations.

3.2 Local event with a maximum frequency of 10 Hz

We applied the same procedure as in Section 3.1 to high-frequency data with a maximum frequency of 10 Hz. The source mechanism, focal depth and location of the stations and of the epicentre are the same as the Friuli event of 1987 studied in Section 4. The earth model Friul7W obtained from the inversion of *P*- and *S*-wave arrival times (Mao & Suhadolc 1992) is used. For this example, the maximum allowed deviations of the initial model from the 'true' model are about $\delta\xi = 30°$, $\delta\eta = 20°$, $\delta\lambda = 30°$ $\delta h = 0.2$ km, $\delta\Delta = 0.5$ km. Fig. 4 shows the inverted results of the fourth iteration, where the initial model being $h = 7.26$ km, $\xi = 199°$, $\eta = 60°$, $\lambda = 40°$ and $\delta\Delta = 0.5$ km. Comparing this with the previous example, we found that the sensitivity of the method to the starting model, in particular to initial centroid parameters, is frequency dependent. The two examples show that the initial location can be in error by approximately the *P*- or *S*-wave wavelength and the initial source mechanism parameters can differ considerably from the 'true' model, their typical deviation ranging between 30° and 40° for strike and rake, and 20° for dip.

3.3 Effects of the earth-model error on the inversion

The determination of source parameters depends upon the earth model used in the inversion. Up to now, we have not found any quantitative description of the relation existing between the inverted source parameters and the earth models used. To obtain such a relation is quite a difficult task, since one would have to account for too many parameters in the inversion process. In the following, we give an example of how the solution obtained depends on the fact that the assumed earth model is never equal to the true one.

To neglect the effects of the Earth's structure beneath the lithosphere, again we work on the local event shown in Section 3.2. The 'observed' signals are generated by the model Friul7W, and the Green's functions used in the inversion are computed by the model Friul7A of Panza & Suhadolc (1987). For details see also Florsch *et al.* (1991)

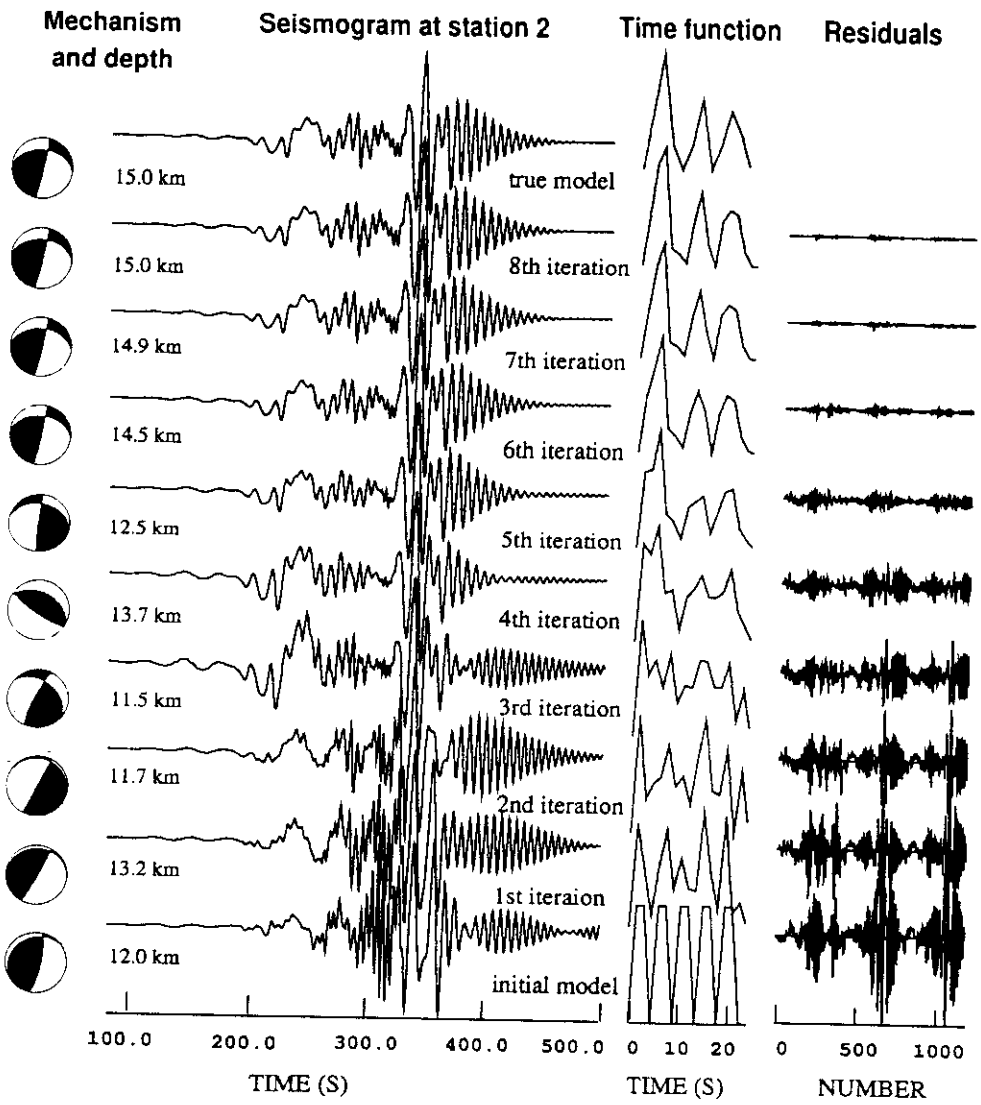

Figure 3. Iterative procedure for source parameters, waveforms and residuals.

and Sileny *et al.* (1992). The two models differ only in their crustal part (upper 30 km). Since the velocities of Friul7A are faster than those of Friul7W in the crust, we have to assume the initial focal depth to be deeper than the 'true' one to have the phase arrival errors less than a period of dominant wave. But, because there are big differences in epicentral distances between the stations, we are not able to have a focal depth which fits for all stations under 1-D structure assumption. Here we use the waveforms of three stations RCL, BAD and ZOU and assume the initial focal depth to be at 10.5 km, and the other initial model parameters to be same as those in Section 3.2. The computed signals (labelled A in Fig. 5) are very different from the 'observed' ones (labelled B), the reason being due to both the differences in the source parameters and in the earth models. After five iterations we obtain a set of signals (labelled C in Fig. 5), which has a minimum residual.

The inverted epicentre location differs by only 0.1 km from the 'true' one, and the source geometric parameters do not show a large deviation from the correct values. The inverted depth and source-time function, on the other hand, show significant differences with respect to the 'true' solution. The source depth is 3.33 km deeper than the 'true' one, i.e. is affected by an error of about 50 per cent, and the peak value of the time function is delayed by about 0.25 s. The delay of the peak of the source-time function and deeper source location compensate to some extent for the decrease in traveltime due to the use of a too fast structural model. The inverted seismic moment is less than the 'true' one by about 35 per cent. This is probably due to the difference in the attenuation models (the model Friul7W has much lower Q values in the upper crust with respect to the model Friul7A) and to the fact that seismic waves lose more energy during their propagation in the model Friul7W, especially at the high-frequency band. Therefore, this example indicates that the effect of the crustal model on the source mechanism is not important, but there are the trade-offs between crustal model, focal depth and

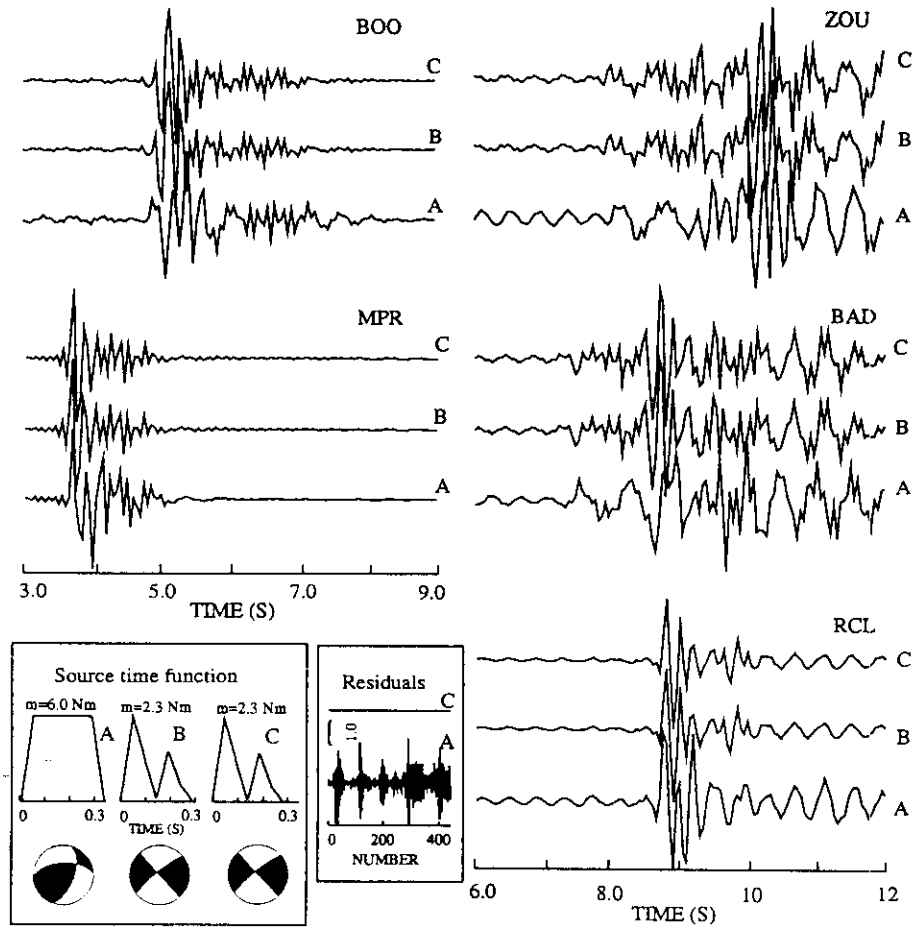

Figure 4. Same as Fig. 2 for a local event with the maximum frequency of 10 Hz; the position of stations and source location are shown in Fig. 7.

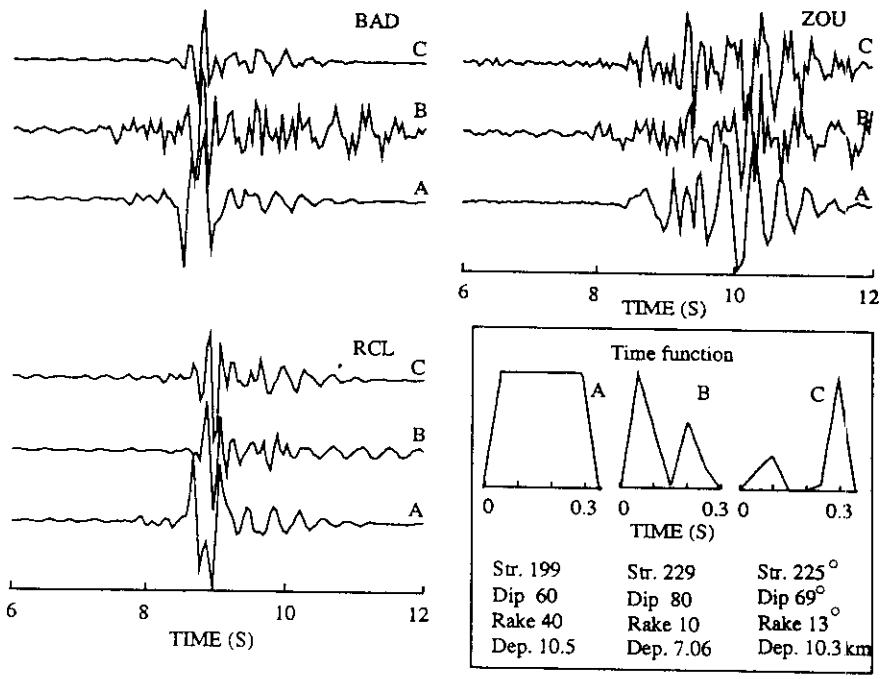

Figure 5. Same as Fig. 2 for synthetic test, considering different crustal structures. The position of stations and source location are shown in Fig. 7 (see text for details).

source-time function. The incorrect earth model can be easily identified by comparing arrivals at the stations used in the inversion.

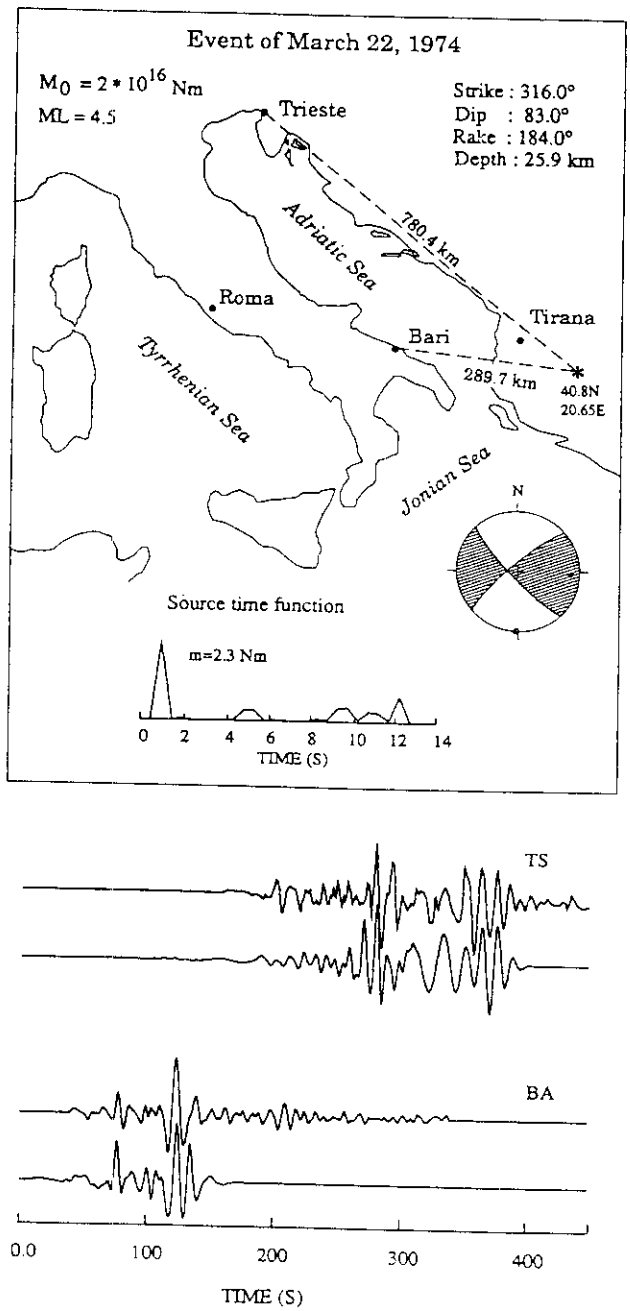

Figure 6. Waveform comparison, inverted source parameters and stations locations for the near-regional event that occurred on 1974 March 22 in Albania. The observed data (upper trace) are bandpass filtered in the band 1/60 Hz, and 1 Hz. The seismograms (lower trace) are computed using the inverted source parameters and the earth models shown in Tables 1 and 2. The asterisk denotes the epicentre. The data recorded at the Trieste and Bari LP (like WWSSN) stations are used. The initial strike, dip, rake and depth are 380°, 70° 196° and 27 km, respectively. The initial source-time function is parametrized by using 25 partly overlapping triangles (see text) with recursive weights (1.0, 1.0, 0.0).

Table 2. Crustal and upper mantle structural model DALMAZ1, $Q_p = 2.5Q_s$.

Thickness (km)	Density (g/cm^3)	P-wave velocity (km/s)	S-wave velocity (km/s)	Q_s
1.0	2.30	4.15	2.40	30.0
9.0	2.32	4.50	2.60	80.0
5.0	2.39	5.20	3.00	300
5.0	2.53	5.54	3.20	300
5.0	2.61	5.89	3.40	300
5.0	2.61	6.24	3.60	300
5.0	2.58	6.58	3.80	300
5.0	2.58	6.93	4.00	300
15.0	2.73	7.27	4.20	300
10.0	2.92	7.79	4.50	300
90.0	3.25	8.17	4.70	300

4 APPLICATION TO OBSERVED DATA

We first apply our inversion procedure to a near-regional ($1° < \Delta < 10°$) $M = 4.5$ event that occurred on 1974 March 22 in Albania and was recorded on the vertical-component LP seismographs of Bari and Trieste (Fig. 6). Since the propagation path from the earthquake source to each of the two stations crosses quite different tectonic settings, we have used two different structural models in the inversion. To compute the synthetic signals at the Bari LP station the South Adriatic model (Table 1) is used, while the synthetic signals at Trieste are computed using a Dalmatia (Croatia) model (Table 2). Both modcels are obtained from the inversion of surface-wave dispersion data (Calcagnile *et al.* 1982; Cragleitto *et al.* 1989).

The responses of the two seismographs are convolved with the theoretical seismogram before the inversion, and the data are bandpass filtered in the frequency band ranging from 1/60 Hz to 1 Hz. The fault-plane solution obtained by D'Ingeo, Calcagnile & Panza (1980) using *P* and *PKP* phases is used for the initial source parameters. The source-time function is modelled by 25 triangles with $\delta t = 1$ s and $\delta\tau = 0.4882$ s, the last value being equal to the sampling rate of the theoretical seismograms.

After six iterations the rms error reaches a minimum and the solution obtained is reported in Fig. 6, which shows that the observed and theoretical waveforms match quite closely. The focal mechanism of the event is of the strike-slip type, and is similar to the result obtained from *P*-wave polarities by D'Ingeo *et al.* (1980). The inverted epicentre and focal depth are, respectively, about 10 km and 1 km away from the initial ones. From the source-time function one can observe that, in the frequency band analysed, most of the energy was released in the first 2 s. The 0.5 s delay prior to the significant moment release probably represents a compensation for the average velocity error in the used models. The seismic moment, M_0, given by eq. (20) is about 2×10^{16} Nm, which, according to the formula $M = \frac{2}{3}\log M_0 - 6.0$ (Hanks & Kanamori 1979, modified), corresponds to a magnitude 4.5.

The procedure has been further tested considering a local ($\Delta < 1°$) $M_l = 2.9$ event that occurred on 1987 December 27 in Friuli (NE Italy). This earthquake was recorded at five local vertical-component SP stations of the Friuli seismic network (Fig. 7). The observed seismograms are low-pass filtered with a cut-off frequency at 10 Hz. At high

frequencies ($f > 1$) the adequacy of the crustal Green's functions to describe wave propagation becomes a critical assumption. The observed Friuli event contains dominant waves of 5–8 Hz, which implies that the crustal structure must be known at wave lengths of approximately 0.5 km for mid-crustal velocities in Friuli. In this test, we use the model Friul7W obtained from the inversion of *P*- and *S*-wave arrival times (Mao & Suhadolc 1992). Although the original inverted model consisted of a set of layered structure of 3–5 km thickness, it was split into a thinner layer (about 0.5 km) gradient structure in terms of studies on the synthetic waveforms in the Friuli area (Mao *et al.* 1990). This model works very well in producing synthetic seismograms which accurately model the high-frequency data (Florsch *et al.* 1991; Sileny *et al.* 1992). In order to demonstrate that the model Friul7W can generate high-frequency waves which are greater than 5 Hz, we computed synthetic seismograms with a relatively simple triangular time function with a duration of 0.1 s, using the source–stations distribution and source parameters in Fig. 7. The synthetic waveforms and their frequency spectra show clearly high-frequency wave propagation (Fig. 8). The initial source location obtained from program HYPO71 (Lee & Lahr 1975), and the *P*-wave fault-plane solution, obtained on the basis of known first-motion polarities (Brillinger, Udias & Bolt 1980; Buforn 1982), are used as initial source parameters. The source-time function is modelled by 20 triangles with $\delta t = 0.1$ s and $\delta\tau = 0.04882$ s.

After 10 iterations the solution shown in Fig. 7 has been obtained. The inverted seismograms (lower trace) are similar to the observed ones for the stations MPR, BOO and BAD, but the fit for the stations RCL and ZOU, which are the farthest from the epicentre, is not as good as for the three closest stations. This might be attributed to possible differences in the structural model and/or to lateral heterogeneities in the crust. We give the amplitude spectra

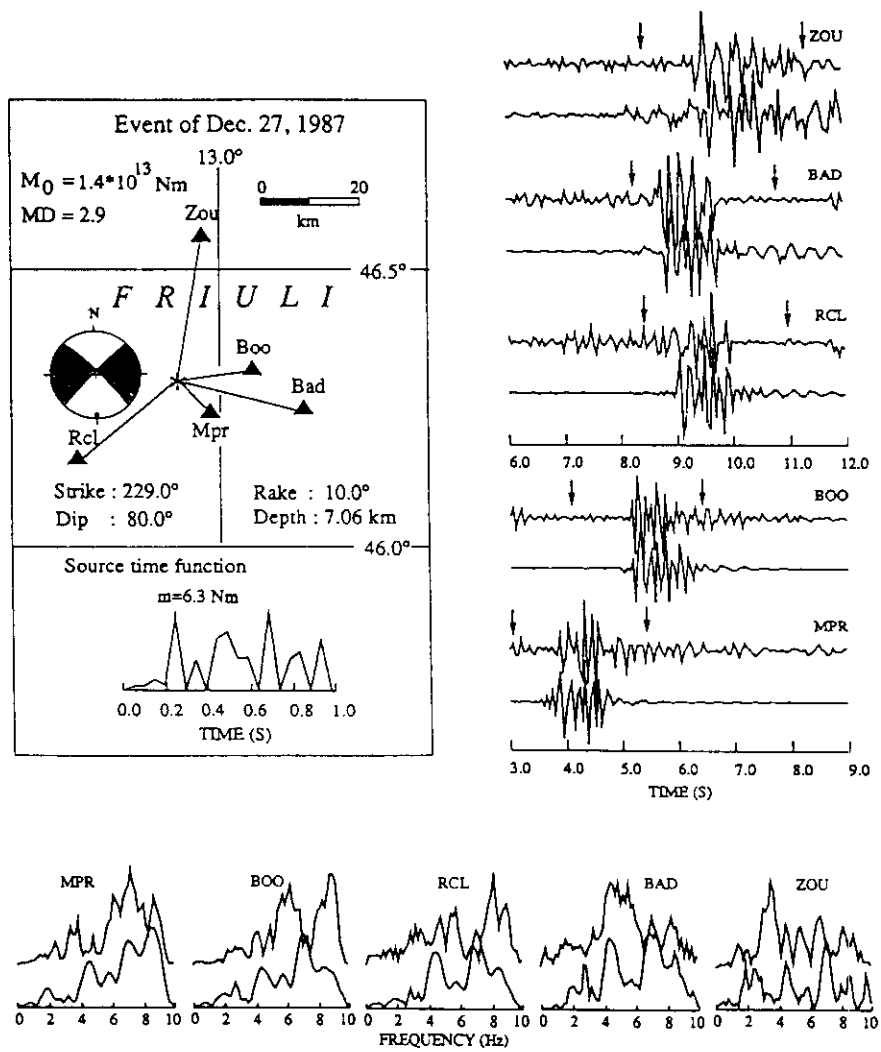

Figure 7. Waveform and amplitude spectrum comparison, inverted source parameters and station locations for the local event that occurred on 1987 December 27 in Friuli (NE Italy). The observed data (upper trace) are low-pass filtered with a cut-off frequency at 10 Hz. The seismograms (lower trace) are computed using the inverted source parameters and the earth model Friul7W. The asterisk denotes the epicentre. The data recorded at the five stations denoted by full triangles are used. The initial strike, dip, rake and depth are 259°, 71°, 46° and 7.1 km, respectively. The initial source-time function was parametrized by using 20 triangles with recursive weights (0.0, 0.0, 1.0). The arrows denote the time window used in the inversion.

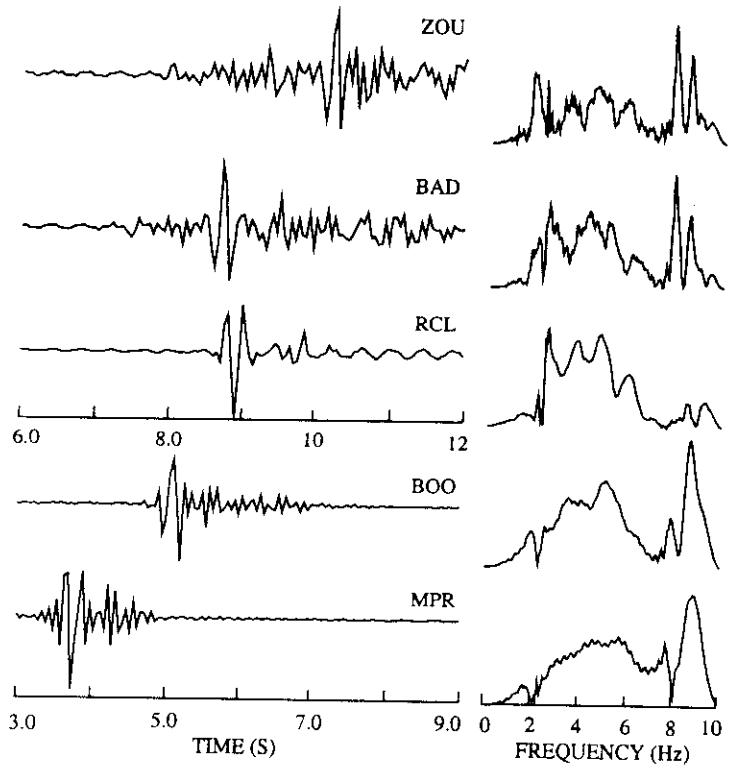

Figure 8. Synthetic seismograms and amplitude spectra with a simple triangular time function with a duration of 0.1 s, the source–stations distribution and source parameters are shown in Fig. 7.

of the inverted and observed waveforms in Fig. 7. They also show good fit. The focal mechanism of this local event is of the strike–slip type. The source mechanism given by the inversion is consistent with the first-arrival polarities, and is similar to that obtained by Sileny *et al.* (1992) using a waveform-inversion method for the retrieval of the point-source moment tensor. Also the duration (about 1 s) of the source process is in very good agreement with the results of Sileny *et al.* (1992). Some slight differences might be due to the fact that their source-time function contains some non-double-couple components and that the no-backward slip constraint is imposed only in the final stage of the inversion. The retrieved seismic moment is about 1.4×10^{13} Nm, which is compatible with what was found by Sileny *et al.* (1992), who assign a value of 1.0×10^{13} Nm to this event.

The above results indicate that our method can be used to investigate the source complexity even of small-magnitude events studied at high frequencies (>5 Hz). If the retrieved $\dot{m}(t)$ is considered representative of a complex multiple rupture process, the event consists of at least three subevents each with 0.3 s duration. For a $M_d = 2.9$ event a total source-time duration of 1 s seems, however, too long and would correspond to an unbelievably low stress drop (Archuleta *et al.* 1982), even if we are dealing with time-extended point sources, for which source dimensions and stress drops are of no significance. In fact, since we are using an average 1-D structural model, the later parts of the source-time function $\dot{m}(t)$ are at least partly due to the effect of lateral heterogeneities (Faeh, Suhadolc & Panza 1993), which have not been taken into account in our Green's functions, and partly due to the different surficial geology (site effects under the stations). However, since we average the $\dot{m}(t)$ over the five stations, we are minimizing these effects, but we are probably not eliminating them completely. To reduce them further one should use at least the 2.5-D approach (2-D for each source–station path). Anyway, the retrieved source-time function of such local events will never give the true picture of the source process unless the (3-D) structure is known exactly (which is never the case). Since we are using a 1-D structural model, which is an average 1-D model of the area examined, the resulting source-time function cannot be interpreted in an absolute way. In fact, an inversion for the source-time function will always produce a time-varying function, more or less peaked and more or less long. Only if we had several events in the same source area (same source–receiver paths), could we say something about the relative complexity of the inverted source functions.

5 CONCLUSIONS

The method illustrated in this paper allows us to retreive simultaneously the mechanism, location, source-time function and seismic moment of seismic sources from broad-band waveform data of local and near-regional events even when few records are available. The basic assumption, quite reasonable for tectonic earthquakes, is that the source mechanism is a double-couple with zero moment. Since we

are able to use structures appropriate for each source–station path and use the full waveform information (both phases and amplitudes) to obtain the source parameters, provided the structural information is available, the method should give results of higher quality with respect to those obtained by using a simple European structural model (ISC or CSEM determinations) and few polarities. Moreover, fewer stations are sufficient with waveform inversion, which introduces less noise due to the inadequacy of the starting model. The locations derived by waveform inversion do not suffer from the difficulty of phase picking which may introduce errors much larger than the ones due to structural inadequacies.

Since the partial derivatives of the theoretical seismograms with respect to all source parameters can be computed analytically, the computer time used for the inversion is greatly reduced. The use of a weighting matrix and of a damping factor, which is variable in each iteration, avoids the problems typical of ill-conditioned matrix inverses and guarantees the stability of the inverse solution.

The tests with synthetic data indicate that the effect of the crustal model on the source mechanism is not important, but there are trade-offs between focal depth, source-time function and crustal model. If the earth models are adequate, the inversion converges rapidly to the 'true' solution. The sensitivity of the method to the starting model, in particular to initial centroid parameters, is frequency dependent. The initial location can be in error by approximately the *P*- or *S*-wave wavelength and the initial source mechanism parameters can differ considerably from the 'true' model, their typical deviation ranging between 30° and 40° for strike and rake, 20° for dip. Moreover, the retrieved source-time function can be interpreted in terms of source complexity only through a comparison with source-time functions of other events in the same source area (and with same source–receiver paths). In the case of insufficient starting information about an event, one can use a Monte Carlo process with a relatively large sampling interval to obtain a reasonable initial solution vector.

The method has been applied to two earthquakes, a near-regional event that occurred on 1974 March 22 in Albania and was recorded by the vertical-component LP (like WWSSN) seismographs of Bari and Trieste and a local event that occurred on 1987 December 27 in Friuli (NE Italy) and was recorded at five local vertical-component digital short-period stations of the Friuli seismic network. In both cases the iterations converged smoothly to solutions, which are consistent with previous studies.

The method presented in this paper is complementary to that of Sileny *et al.* (1992). The two methods can be used in an iterative procedure in order to obtain successive refined estimates of the location, depth, source-time history, fault-plane solution and an indication of the appropriateness of the structural model used in the computations.

ACKNOWLEDGMENTS

We are grateful to the computer center ENEA INFO BOL for the use of their Bologna IBM3090 computer and Dr M. Russi of Osservatorio Geofisico Sperimentale, Trieste, for supplying the observed data for the 1987 December 27 Fruili (NE Italy), event. We thank the two anonymous referees for some very constructive and critical reviews, which helped to improve the paper. This research has been performed within the framework of the International Lithosphere Programme (ILP) Theme II-4: 'Three-Dimensional Modelling of the Earth's Lithosphere/Asthenosphere (Tectosphere), and of Seismic Sources, in Selected Regions'. This research was funded by CNR grants 91.00198.CT02 and 91.02376.CT12, by MURST 40CEESC1*0176-C(SMA) and by PNRA (Linea 5, tema g1-2). The revised work was completed under AMOCO contract RAD 23(90).

REFERENCES

Aki, K. & Richards, P.G., 1980. *Quantitative seismology*, W. H. Freeman, San Francisco.

Archuleta, R.J., E. Cranswick, C. Mueller, C. & Spudich, P., 1982. Source parameters of the 1980 Mammoth lakes, California, earthquake sequence, *J. geophys. Res.*, **87,** 4595–4607.

Brillinger, D.R., Udias, A. & Bolt, B.A., 1980. A probability model for regional focal mechanism solutions, *Bull. seism. Soc. Am.*, **70,** 149–170.

Buforn, E., 1982. Estuido estadistico de la direccion de esfuerzos principales en terremotos, *Doctoral thesis*, Universidad Complutense, Madrid, Spain.

Burridge, R. & Knopoff, L., 1964. Body force equivalents for seismic dislocations, *Bull. seism. Soc. Am.*, **54,** 1875–1888.

Calcagnile, G., D'Ingeo, F., Farrugia, P. & Panza, G.F., 1982. The lithosphere in the Central-eastern Mediterranean area, *Pageoph*, **120,** 389–406.

Carrion, P.M., 1989. Generalized non-linear elastic inversion with constraints in model and data spaces, *Geophys. J. Int.*, **96,** 151–162.

Craglietto, A., Panza, G.F., Mitchell, B.J. & Costa, G., 1989. Anelastic properties of the crust in the Mediterranean area, *Am. geophys. Un. Geophys. Monogr.* **51,** IUGG, Vol. 6, 179–196.

D'Ingeo, F., Calcagnile, G. & Panza, G.F., 1980. On the fault-plane solutions in the Central-eastern Mediterranean region, *Boll. Geofis. Teor. Appl.*, **21,** 13–22.

Dreger, D. & Helmberger, D.V., 1991. Complex faulting deduced from broadband modeling of the 28 February 1990 Upland eartquake (M_L = 5.2), *Bull. seism. Soc. Am.*, **81,** 1129–1144.

Dreger, D. & Helmberger, D.V., 1992. On the determination of earthquake source parameters from regional and local broadband data, *EOS, Trans. Am. geophys. Un.* (Abstract), **73,** 43.

Dziewonski, A.M., Chou, T.A. & Woodhouse, J.H., 1981. Determination of earthquake source parameters from waveform data for studies of global and regional seismicity, *J. geophys. Res.*, **86,** 2825–2852.

Faeh, D., Suhadolc, P. & Panza, G.F., 1993. Variability of seismic ground motion in complex media: the case of a sedimentary basin in the Friuli (Italy) area. *Int. J. appl. Geophys.*, **30,** 131–148.

Fan, G.W. & Wallace, T., 1991. The determination of source parameters for small earthquakes from a single, very broadband seismic station, *Geophys. Res. Lett.*, **18,** 1385–1388.

Florsh, N., Faeh, D., Suhadolc, P. & Panza, G.F., 1991. Complete synthetic seismograms for high-frequency multimode *SH* waves, in El Escorial Worskshop Proceedings, eds Udias & Buforn, *Pageoph*, **136,** 529–560.

Hanks, T.C. & Kanamori, H., 1979. A moment-magnitude scale, *J. geophys. Res.*, **84,** 2348–2350.

Harkrider, D.G., 1970. Surface waves in multilayered elastic media, Part II—Higher mode spectra and spectral ratios from point

sources in plane layered earth models, *Bull. seism. Soc. Am.*, **60**, 1937–1987.

Haskell, N.A., 1953. Dispersion of surface waves on multilayered media, *Bull. seism. Soc. Am.*, **43**, 17–34.

Langston, C.A., 1981. Source inversion of seismic waveforms: the Koyna, India, Earthquakes of 13 September 1967, *Bull. seism. Soc. Am.*, **71**, 1–24.

Lee, W.H.K. & Lahr, J.C., 1975. HYPO71 (revised): a computer program for determining hypocenter, magnitude, and first motion pattern of local earthquakes, *U.S. Geol. Surv. Open-File Rept*, 75–311.

Mao, W.J. & Gubbins, D., 1993. Simultaneous determination of time delays and stacking weights in seismic array beamforming, *Geophysics*, submitted.

Mao, W.J. & Suhadolc, P., 1992. Simultaneous inversion of velocity structures and hypocentral locations: application to the Friuli seismic area NE Italy, *Pageoph*, **138**, 267–285.

Mao, W.J., Suhadolc, P., Faeh, D. & Panza, G.F., 1990. An example of interpretation strong motion data by source complexity, in *Abstracts of 18th International Conference on Mathematical Geophysics*, Weizmann Institute of Science, Jerusalem, Israel.

Nabelek, J.L., 1984. Determination of earthquake source parameters from inversion of body waves, *PhD thesis*, Massachusetts Institute of Technology.

Panza, G.F., 1985. Synthetic seismograms: the Rayleigh waves model summation, *J. Geophys.*, **58**, 125–145.

Panza, G.F. & Suhadolc, P., 1987. Complete strong motion synthetics, in *Seismic Strong Motion Synthetics, Computational Techniques*, Vol. 4, pp. 153–204, ed. Bolt, B. A., Academic Press, Orlando.

Panza, G.F., Schwab, F. & Knopoff, L., 1973. Multimode surface waves for selected focal mechanisms, I. Dip–slip sources on a vertical fault plane, *Geophys. J. R. astr. Soc.*, **34**, 265–278.

Panza, G.F., Suhadolc, P. & Chiaruttini, C., 1986. Exploitation of broadband networks through broadband synthetic seismograms, *Ann. Geophys.*, **4B**, 315–328.

Ritsema, J. & Lay, T., 1992. Time-domain waveform inversion of long-period regional waveforms, *EOS, Trans. Am. Geophys. Un.* (Abstract), **73**, 43, 375.

Ruff, L. & Kanamori, H., 1983. The rupture process and asperity distribution of three great earthquakes from long-period diffracted *P*-waves, *Phys. Earth planet. Inter.*, **31**, 202–230.

Sileny, J., Panza, G.F. & Campus, P., 1992. Waveform inversion for point source moment tensor retrieval with variable hypocentral depth and structural model, *Geophys. J. Int.*, **109**, 259–274.

Stump, B.W. & Johnson, L.R., 1977. The determination of source properties by the linear inversion of seismograms, *Bull. seism. Soc. Am.*, **67**, 1489–1502.

Vaccari, F., Gregersen, S., Furlan, M. & Panza, G.F., 1989. Synthetic seimograms in laterally heterogeneous anelastic media by modal summation of *P–SV* waves, *Geophys. J. Int.*, **99**, 285–295.

Walter, W.R., 1992. Source parameters of the June 29, 1992 little Skull mountain earthquake from complete regional waveforms at a single station, *EOS, Trans. Am. geophys. Un.* (Abstract), **73**, 43, 375.

APPENDIX: COMPUTATION OF THE PARTIAL DERIVATIVES OF THE THEORETICAL SEISMOGRAM WITH RESPECT TO SOURCE PARAMETERS

From eq. (2) we see that only the radiation pattern $\chi(\xi, \eta, \lambda, h)$ is a function of the source geometry and depth.

Table A1. Coefficients of the radiation pattern function for a double-couple point source.

coefficient	Love	Rayleigh
d_0	0	(1/2) sinλ sin2η B(h)
d_1	cosλ cosη G(h)	- sinλ cos2η C(h)
d_2	-sinλ cos2η G(h)	- cosλ cosη C(h)
d_3	(1/2) sinλ sin2η V(h)	cosλ sinη A(h)
d_4	cosλ sinη V(h)	-(1/2) sinλ sin2η A(h)

Following Harkrider (1970),

$$\chi(\xi, \eta, \lambda, h) = d_0 + i(d_1 \sin\xi + d_2 \cos\xi) + d_3 \sin 2\xi + d_4 \cos 2\xi, \quad \text{(A1)}$$

where the radiation pattern coefficients for a double-couple point source are given in Table A1.

The quantities $A(h)$, $B(h)$, $C(h)$, $G(h)$ and $V(h)$ are given in terms of the Thomson–Haskell normalized displacement-stress vector elements (Haskell 1953; Harkrider 1970) as

$$\begin{aligned} A(h) &= -[u_S^*(h)/w(0)], \\ B(h) &= -[[3 - 4(\beta_S^2/\alpha_S^2)][u_S^*(h)/w(0)] \\ &\quad + [2/(\rho_S\alpha_S^2)]\{\sigma_{RS}^*(h)/[\dot{w}(0)/c_R]\}], \\ C(h) &= -(1/\mu_S)\{\tau_{RS}(h)/[\dot{w}(0)/c_R]\}, \\ G(h) &= -(1/\mu_S)\{\tau_{LS}^*(h)/[\dot{v}(0)/c_L]\}, \\ V(h) &= [v_S(h)/v(0)], \end{aligned} \quad \text{(A2)}$$

where ρ is the denstiy, μ is the rigidity, α is the P-wave velocity, β is the S-wave velocity, c is the phase velocity; the subscript S denotes quantitites evaluated at the source depth; the subscripts R and L denote quantities associated with Rayleigh and Love modes, respectively.

Table A2. Partial derivatives of the coefficients of the radiation pattern function.

∂/∂η	Love	Rayleigh
d_0	0	sinλ cos2η B(h)
d_1	- cosλ sinη G(h)	2 sinλ sin2η C(h)
d_2	2 sinλ sin2η G(h)	cosλ sinη C(h)
d_3	sinλ cos2η V(h)	cosλ cosη A(h)
d_4	cosλ cosη V(h)	- sinλ cos2η A(h)

∂/∂λ	Love	Rayleigh
d_0	0	(1/2) cosλ sin2η B(h)
d_1	- sinλ cosη G(h)	- cosλ cos2η C(h)
d_2	- cosλ cos2η G(h)	sinλ cosη C(h)
d_3	(1/2) cosλ sin2η V(h)	- sinλ sinη A(h)
d_4	- sinλ sinη V(h)	-(1/2) cosλ sin2η A(h)

From eqs (A1) and (A2) and Table A1, we have

$$\partial\chi/\partial\xi = i(d_1 \cos\xi - d_2 \sin\xi) + 2d_3 \cos 2\xi - 2d_4 \sin 2\xi. \tag{A3}$$

The partial derivatives of the radiation pattern with respect to η and λ are given in Table A2.

The partial derivatives of the displacement-stress quantities with respect to the source depth are (Harkrider 1970)

$$(\partial/\partial h)[u_S^*(h)/w(0)] = k_R[[w_S(h)/w(0)] + (1/\mu_S)\{\tau_{RS}(h)/[\dot{w}(0)/c_R]\}],$$

$$(\partial/\partial h)\{\sigma_{RS}^*(h)/[\dot{w}(0)/c_R]\} = k_R[\rho_S c_R^2[w_S(h)/w(0)] + \{\tau_{RS}(h)/[\dot{w}(0)/c_R]\}],$$

$$(\partial/\partial h)\{\tau_{RS}(h)/[\dot{w}(0)/c_R]\} = -k_R[\lambda_S/(\lambda_S + 2\mu_S) \times \{\sigma_{RS}^*(h)/[\dot{w}(0)/c_R]\} + \{\rho_S c_R^2 - [4\mu_S\lambda_S + \mu_S)/(\lambda_S + 2\mu_S)]\} \times [u_S^*(h)/w(0)]], \tag{A4}$$

$$(\partial/\partial h)\{\tau_{LS}^*(h)/[\dot{v}(0)/c_L]\} = k_L(\rho_S c_L^2 - \mu_S)[v_S(h)/v(0)],$$

$$(\partial/\partial h)[v_S(h)/v(0)] = -(k_L/\mu_S)\{\tau_{LS}^*(h)/[\dot{v}(0)/c_L]\},$$

where k is the wavenumber.

Geophys. J. Int. (1992) **109**, 259–274

Waveform inversion for point source moment tensor retrieval with variable hypocentral depth and structural model

J. Šílený,[1] G. F. Panza[2,3] and P. Campus[2]

[1] *Geophysical Institute, Czech. Acad. Sci., Bocni II, 14131 Praha 4, Czechoslovakia*
[2] *Università di Trieste, Istituto di Geodesia e Geofisica, Via dell'Università 7, 34123 Trieste, Italy*
[3] *International Institute for Earth, Environmental and Marine Sciences and Technologies, Via Beirut 7, 34100 Trieste, Italy*

Accepted 1991 November 7. Received 1991 November 4; in original form 1990 February 12

SUMMARY

In the inversion scheme of high-frequency seismograms, recorded by a local network, we have developed the unconstrained moment tensor description to study weak events which are believed to reflect small-scale complexities of the tectonic structure. In order to allow the source mechanism to change with time each moment tensor component has its own time history. In the inversion, the measure of the similarity between the synthetic seismograms and the observed records is obtained by minimizing the norm L_2 of their difference. The initial synthetic seismograms are constructed by summing a set of time-dependent functions, named base functions. These base functions are computed by normal mode summation for a discrete set of source depths and for two structural models, considered to represent acceptable extremes for the region under study. In the course of the inversion, using a linear interpolation, new base functions are computed for intermediate values of the starting depths and structures. Thereafter new synthetic seismograms are computed and compared with the observed records until the convergence is reached, within some pre-assigned threshold for the norm L_2.

The method has been tested by treating, as 'observed' records, synthetic seismograms (both displacement and velocity) generated for instantaneous and finite duration sources. The 'observed' records have been computed for two structures: one belonging to the structural range within which the base functions were computed, the other lying outside this range. Random noise has been superimposed on the records.

When inverting synthetic records computed for a structure contained within the range of interpolation for the base functions, the full moment tensor is retrieved satisfactorily (provided that the noise level does not exceed about 20 per cent). For records computed for a structure lying outside this range a spurious volumetric part of the moment tensor appears. However, if the volumetric part of the moment tensor is removed, the source time function can be reconstructed satisfactorily, and the source mechanism can be determined from the deviatoric part of the moment tensor.

The procedure has been applied to vertical component seismograms recorded in the Friuli (NE Italy) area for the $M_L = 2.9$ event of 1987 December 27. The retrieved source mechanism is in agreement with the distribution of the few first arrival polarities available and the source time function indicates a possible multiple rupture process.

Key words: modal summation, source mechanism, time function, waveform inversion.

1 INTRODUCTION

Since the pioneering paper of Gilbert & Dziewonski (1975), who inverted free-oscillation data to retrieve the source moment tensor of large earthquakes, many approaches have been proposed to study the earthquake source by inverting waveforms. The models of the source and the methods used differ greatly according to the purpose of the study and the data used. Here the seismograms observed in the stations of a local network (the distances between stations are roughly tens of kilometres) are considered. For such configurations sophisticated inversions for finite source models have been performed provided that strong earthquakes were treated (e.g. Hartzel & Heaton 1983; Ohlson & Apsel 1982; Frankel & Venneberg 1989). Our aim is to investigate weak events, therefore we concentrate on the point source approximation. In our description of the rupture process the source is allowed to act during a finite time interval. This description may appear to be inconsistent for local event investigation, since the orders of space and time source moments are different (Bukchin 1990, personal communication). However, when treating weak local events, this assumption is acceptable. In fact by using records from the distances mentioned it is not possible to resolve the internal space structure of the source, but it is in any case possible to recognize subsequent energy releases. Effects generated by possible rupture spreading in the focal zone are transformed into complexities of the point source time function. From this viewpoint the approach followed here resembles source studies performed by using teleseismic data (e.g., Mendiguren 1977; Kikuchi & Kanamori 1982; Trehu, Nabelek & Solomon 1981; Sipkin 1982; Nabelek 1984). However, compared to teleseismic cases, where either the hypocentre is fixed or is allowed to change in a given velocity model only, our approach is more general. Both the depth of the source and the structural model representing the area in which the event occurred are permitted to vary in an *a priori* chosen range. This is done because the source depth strongly influences the waveforms and the precision with which this source parameter is determined with standard procedures is generally not satisfactory; for similar reasons we have allowed changes in the structural parameters. A preliminary study along these lines has been performed by Šílený & Panza (1991), but with the additional constraints of fixed hypocentral depth and structure.

As the mechanisms of weak events are believed to reflect small-scale complexities of the focal zone, in principle a more general mechanism than a pure shear slip can be expected. Therefore no *a priori* constraint of double couple mechanism is imposed. The source is described by the full moment tensor $M_{ij}(t)$, which can be decomposed in a volumetric component, representing an explosive or implosive movement, and in a deviatoric part, containing both the double couple and the compensated linear vector dipole (CLVD) components. This latter, like the double couple part, does not imply a change in the source volume and corresponds to three vector dipoles without moment; one of them is double in modulus with respect the others (Jost & Herrmann 1989).

2 THEORETICAL BACKGROUND

The method consists of two steps: (1) linear waveform inversion of the source parameters for fixed source depth and structural model; and (2) subsequent perturbation of the source depth and structural parameters. These two steps are iterated until the convergence between observed and computed records is reached, within a pre-assigned threshold for the L_2-norm of their difference.

2.1 Linear inversion

The source is described in the space-point approximation with the moment tensor representation, by means of which the kth component of the displacement field can be expressed as a convolution of the moment tensor with the space derivative of the Green functions $G_{ki,j}(t)$ (e.g., Aki & Richards 1980):

$$u_k = \sum_{i,j=1}^{3} M_{ij}(t) * G_{ki,j}(t). \tag{1}$$

The values $G_{ki,j}(t)$ are the responses of the medium to sources represented by elementary dipoles with the time dependence given by a δ-function. For a seismic source it is reasonable to consider an increasing time function $M_{ij}(t)$ with an asymptote, i.e. the time derivatives of this function, $\dot{M}_{ij}(t)$, are non-zero in a limited interval only. These time derivatives of the moment tensor components are more convenient for the parametrization than the functions $M_{ij}(t)$ themselves, therefore it is advantageous to write (1) as

$$u_k = \sum_{i,j=1}^{3} \dot{M}_{ij}(t) * H_{ki,j}(t), \tag{2}$$

where $H_{ki,j}(t)$ are the responses of the medium to sources represented by elementary dipoles with the time dependence given by a Heaviside function. In the following the functions $H_{ki,j}(t)$ will be called base functions, and will be explicitly computed using the multimode summation method (Panza 1985).

For the sake of convenience, let us introduce the notation

$$\dot{M}_{ij} \rightarrow F_m, \qquad i, j = 1, 2, 3, \; m = 1, \ldots, 6,$$

$$H_{ki,j} \rightarrow \Phi_{km}, \qquad i, j, k = 1, 2, 3, \; m = 1, \ldots, 6.$$

Then (2) can be rewritten as

$$u_k(t) = \sum_{m=1}^{6} F_m(t) * \Phi_{km}(t). \tag{3}$$

Let us parametrize each derivative of the moment tensor components $F_m(t)$ by means of time-delayed overlapping triangles of half-width $\Delta\tau$ and of unit height, the time delay being equal to $\Delta\tau$. Each triangle is obtained as a convolution of two box functions of length $\Delta\tau$ (Nabelek 1984):

$$T_{\Delta\tau}(t) = \frac{1}{\Delta\tau} B_{\Delta\tau}(t) * B_{\Delta\tau}(t),$$

where

$$B_{\Delta\tau}(t) = 1 \quad \text{for } 0 \le t \le \Delta\tau,$$

$$B_{\Delta\tau}(t) = 0 \quad \text{elsewhere.}$$

If Nt is the number of these triangles, it can be written

$$F_m(t) = \sum_{n=1}^{Nt} F_{nm} T_{\Delta\tau}[t - (n-1)\,\Delta\tau], \tag{4}$$

where F_{nm} is the weight of the nth triangle in the parametrization of the mth moment tensor component, or, equivalently, F_{nm} is the geometrical part of the nmth component of the moment tensor at each instant $t_n = (n-1)\,\Delta\tau$. The F_{nm} components at a given time t_n give the fault plane solution at this time. Inserting (4) into (3) yields

$$u_k(t) = \sum_{m=1}^{6} \sum_{n=1}^{Nt} F_{nm} T_{\Delta\tau}[t-(n-1)\,\Delta\tau] * \Phi_{km}(t). \tag{5}$$

We compress the indexes m and n by introducing an index p

$$p = m + 6(n-1), \tag{6}$$

which results in simplification of (5) in the form

$$u_k(t) = \sum_{p=1}^{6Nt} w_p A_{kp}(t), \tag{7}$$

where w_p corresponds to F_{nm}, therefore the vector

$$\mathbf{w} = (F_{11}, \ldots, F_{16}, F_{21}, \ldots, F_{26}, \ldots, F_{Nt,1}, \ldots, F_{Nt,6}),$$

containing the parameterization weights can be defined, and $A_{kp}(t)$ corresponds to $T_{\Delta\tau}[t-(n-1)\,\Delta\tau] * \Phi_{km}(t)$. Each set of weights $(F_{n1}, \ldots, F_{n6})$ represents the geometrical part of the moment tensor corresponding to the nth triangle. Let $d_k(t)$ be the kth component of the observed record: the unknown weights w_p are determined by solving the equations

$$\sum_{p=1}^{6Nt} w_p A_{kp}(t) = d_k(t), \tag{8}$$

concatenated for all components in all stations of the network. This system of equations can be written in the compact form

$$\mathbf{Aw} = \mathbf{d}, \tag{9}$$

where $\mathbf{A}$ is the matrix containing the sampled functions (7) and $\mathbf{d}$ is a vector of concatenated sampled observed records. The least-squares solution of (9) is obtained by solving the normal equations

$$(\mathbf{A}^{\mathrm{T}}\mathbf{A})\mathbf{w} = \mathbf{A}^{\mathrm{T}}\mathbf{d}, \tag{10}$$

which is a system in $6Nt$ equations for $6Nt$ unknown weights w_p. The arranging of the weights F_{nm} into the vector $\mathbf{w}$ following the ordering (6) gives to the matrix $\mathbf{A}^{\mathrm{T}}\mathbf{A}$ the special form of a 'block-Toeplitz' matrix: $\mathbf{A}^{\mathrm{T}}\mathbf{A}$ is composed of Nt (6×6) submatrices. Such a system of equations can be conveniently solved by means of recursive techniques (e.g., Robinson 1967) which allows us considerable saving of computer time and space. Once the weights w_p have been determined, the synthetic seismograms (7) are computed and compared with the observed records. As a quantitative measure of the similarity between synthetic seismograms and observed records, the least-squares norm of their difference is accepted. The representation of the weights w_p as a function of time gives the time evolution of the geometrical part of the moment tensor component $[M_{ij}(t)]$, i.e. the variation in time of the focal mechanism.

The procedure is very close to that of Sipkin (1982); the difference consists in the introduction of the parametrization of the time functions $F_m(t)$. An additional extension is the possibility to multiply in the system (9) the equations (8), corresponding to particular stations, by different weights. This can be useful to enhance the stations with small recorded amplitudes (due to the radiation pattern) or to decrease the weight of the signals recorded with low quality.

2.2 Extension to treat variable source depth and structural model

The base functions, computed with the multimodal summation method, are generated initially for:

(i) a set of values of the source depth lying between two extremes chosen on the grounds of the uncertainty of the hypocentral location based on P- and S-wave arrivals; and

(ii) two structural models representing reasonable extreme models for the region under study; in the following we will denote these models with A and B.

Let us indicate the different values of the source depth with different values of variable X and let us introduce the parameter Y ($0 \leq Y \leq 1$) to represent the different structural models: when $Y = 0$, the structure used to compute the base functions is A, and when $Y = 1$ the considered structure is B. The structures corresponding to the values of the variable Y in the range $[0, 1]$ are more similar to A if $Y < 0.5$, and more similar to B if $Y > 0.5$. In the course of the inversion intermediate values of the parameters X and Y are computed, incrementing the initial values usually taken equal to 0.5 with steps chosen *a priori*. The base functions corresponding to intermediate values of depth and structure are computed by linearly interpolating the base functions evaluated for the assumed set of depths and structures. Let D be the L_2-norm of the difference between the observed records and the synthetic seismograms computed by means of the base functions corresponding to a given source depth and structural model. The norm D can be treated as a function of the two parameters X and Y and its minimum can be searched by using software designed for function minimization. Here the MINUIT program, written by CERN Computer Centre (CERN Computer Centre Program Manual 1985) is used.

3 TEST ON SYNTHETIC DATA

To prove the ability of the method to retrieve time-dependent moment tensors by matching observed and theoretical seismograms with simultaneous hypocentral depth adjustment and structural model interpolation, a series of synthetic tests is performed.

The base functions are interpolated between the responses constructed for rather different structural models, A and W, of the Friuli area, consistent with independent observations (see Figs 1a and b). The inversion is performed considering both ground displacement and velocity for a local network composed of four vertical component stations, all at the same epicentral distance of 15 km, with azimuths of 20°, 110°, 200° and 290°.

The source used for generating the 'observed' records is a pure shear slip, with dip 45°, strike 50° and rake 30°, situated at a depth of 0.7 km in the first test, and 6.2 km in the latter.

Two sets of 'observed' seismograms having different content of high frequencies are computed. The first set

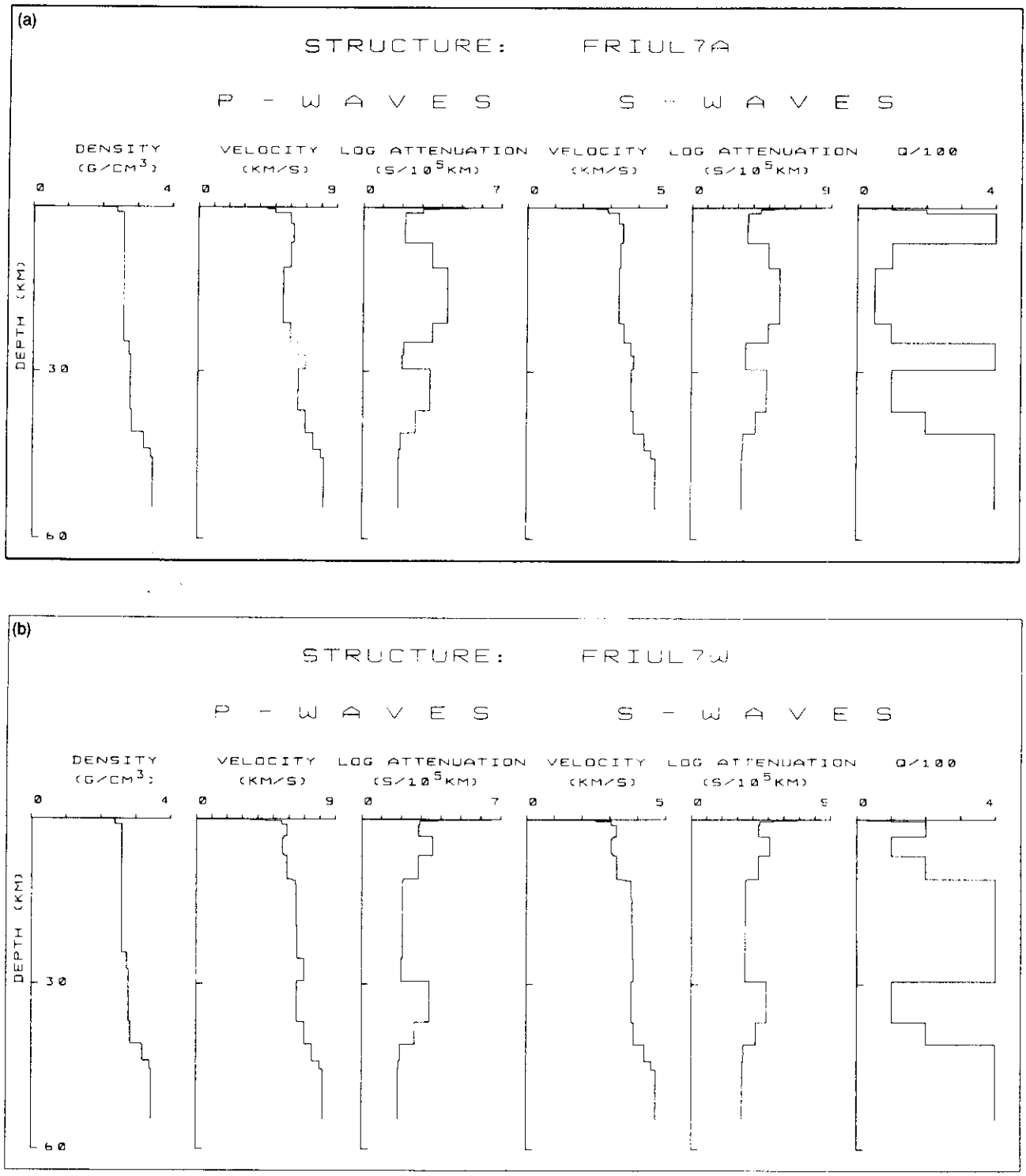

Figure 1. Structural models, for the Friuli region, used in this study. (a) Model FRIUL7A, (b) model FRIUL7W, (c) model FRIUL7R.

corresponds to an instantaneous source, the other to a source with a triangular time function derivative with a duration of 0.6 s.

In the inversion of the 'observed' seismograms generated by an instantaneous source, the source time function was, of course, parametrized with time-delayed triangles of half-width $\Delta\tau$ equal to the sampling step, Δt, of the data ($\Delta t = 0.0488$ s). When using the 'observed' seismograms generated by a time-extended source, the frequency content of the data permits us to use, in the parametrization of the source time function, triangles with a half-width larger than 0.0488 s; we have chosen $\Delta\tau = 2\,\Delta t = 0.0976$ s. In practice

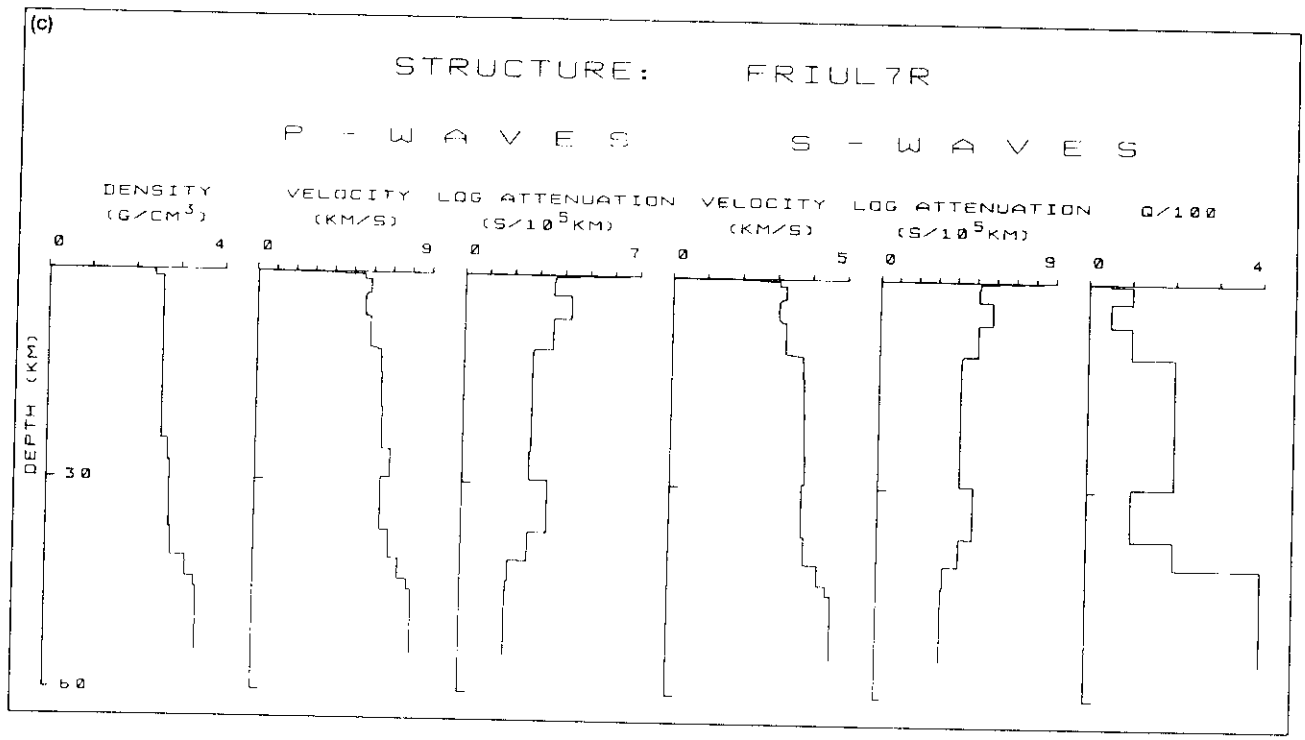

Figure 1. *(continued)*

the choice of $\Delta\tau$ can be made on the basis of the frequency content of the available records.

3.1 Inversion of 'observed' records corresponding to the structure W and to a very shallow source.

The first inversion is performed in the depth range 0.5–1.5 km using 'observed' ground displacements constructed for a structural model contained in the range of the parameter Y. The records for instantaneous and finite duration sources are shown in Figs 2(a) and (b) (thick lines), respectively. The inversion procedure converges very well for both the steps used in the depth discretization and yields synthetic seismograms of nearly identical shape as the 'observed' records. We show only the results of the test performed by using base functions computed with the depth discretization step of 0.5 km (Figs 2a and b, dashed lines).

The best agreement between synthetic seismograms and 'observed' records is obtained by using the structural model corresponding to or very near to the value $Y = 1$. This

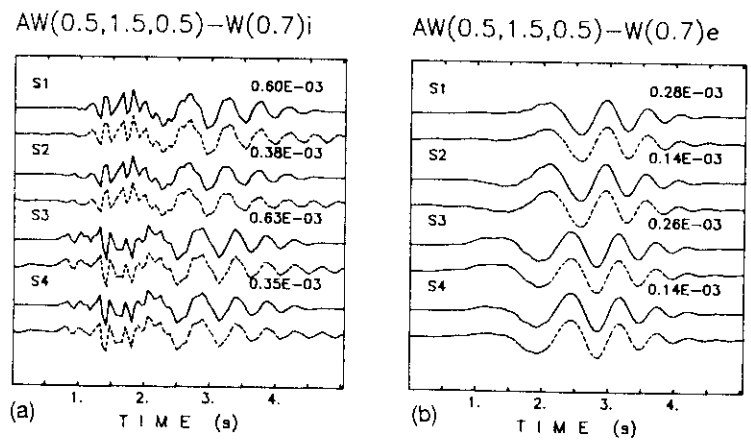

Figure 2. 'Data' (solid lines) and synthetic seismograms (dashed lines) obtained in the inversion with base functions interpolated between the structures FRIUL7A (A) and FRIUL7W (W) and with 0.5 km grid spacing for depth discretization. The heading of each plot indicates the extreme structures, AW; the depth interval (first two numbers) and its discretization step (0.5, 1.5, 0.5); the structure used to compute the 'real record' (W); the depth at which the 'real' records have been computed (0.7); and the source duration (i = instantaneous, e = extended in time). The synthetic displacements used as 'real' data are generated by an instantaneous point source (a) and by a source with a duration of 0.6 s (b) acting in the structural model W. Source parameters: depth 0.7 km, dip 45°, strike 50°, rake 30°. The four stations are situated at a distance of 15 km from the source at the azimuths 20°, 110°, 200° and 290°. The number on the right-hand side of each seismogram represents the maximum amplitude (in cm) in the particular station, for a scalar seismic moment M_0 of 10^{20} dyne cm (10^{13} N m).

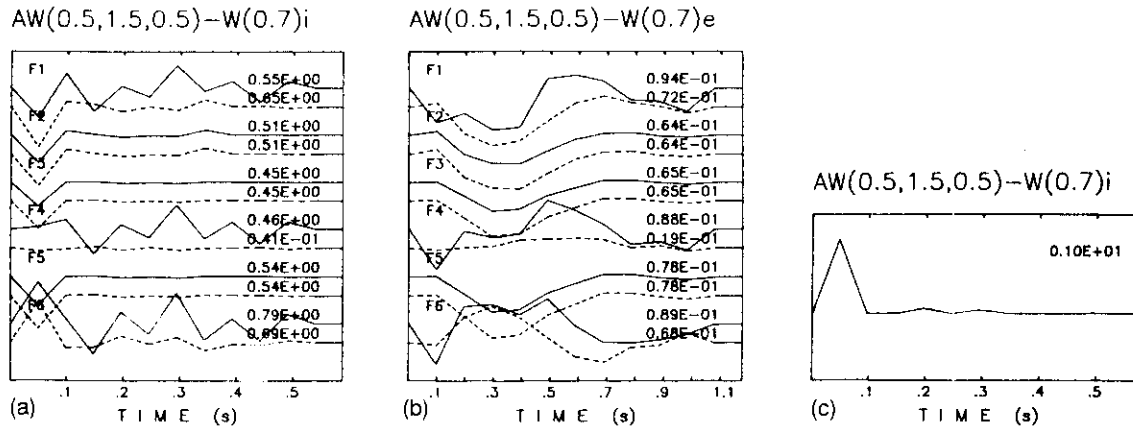

Figure 3. Time functions $M_{ij}(t)$ corresponding to the six moment tensor components obtained from the inversion of the records shown in Fig. 2, by using base functions constructed with a spacing of 0.5 km in the depth interval 0.5–1.5 km. (a) Input solid lines of Fig. 2(a); (b) input solid lines Fig. 2(b). Solid lines represent the $M_{ij}(t)$ functions corresponding to the synthetic seismograms shown in Fig. 2; dashed lines represent the reduced $m_{ij}(t)$ functions (obtained subtracting the volumetric part $[M_{11}(t) + M_{22}(t) + M_{33}(t)]/3$ from $M_{ij}(t)$. The numbers in the right-hand side of each trace indicate the maximum amplitudes of the functions (in units of 10^{20} dyne cm). (c) Joint time function, constrained between 0 and 1.

means that the structural model W is also well resolved. The retrieval of the source depth is not so good: when using the interpolation between base functions computed with a depth spacing of 0.5 km, the source is located at a depth of 0.79 km for the high-frequency records (instantaneous source) and the value of Y is 0.99, while for the smooth records (finite duration source) the hypocentral depth is evaluated at 0.86 km and the structural parameter Y is 0.97. When using interpolation between base functions computed with the depth spacing of 0.25 km the result is much better for the instantaneous records: the source is located at a depth of 0.72 km, i.e. with an error just above 1 per cent and the value of Y is 1. For the smooth records the source is located at a depth of 0.71 km and the retrieved structure corresponds to the value $Y = 1$.

The focal mechanism and its time history are given by the six independent time functions corresponding to the six moment tensor components (indicated in all the plots as $F_1, \ldots, F_6$). The high-frequency input, inverted by using the interpolation between the base functions computed with a depth spacing of 0.5 km, yields the $M_{ij}(t)$ functions plotted in Fig. 3(a). The first peak in all the traces corresponds to an instantaneous source with a mechanism not very far from the true one (see Fig. 4 'true' and Fig. 4a). However, in the subsequent part ($t > 0.2$ s) the functions $M_{ij}(t)$ contain non-zero amplitudes, clearly visible in the records.

The inversion of the smooth records (Fig. 2b) gives nearly the same mechanism as in the previous case (Fig. 4b): the time duration is also well determined (the time duration of the true source is 0.6 s). The inversion of these data is affected by the rough depth discretization but the source duration can still be correctly retrieved to some extent (Fig. 3b).

The inversion performed by using the interpolation between the base functions computed with a depth spacing of 0.25 km, yielding a hypocentral depth very close to the true one, gives $M_{ij}(t)$ functions with a relatively smoother shape for $t < 0.4$ s, but for larger values of t a peak is required to fit the data. The well-pronounced first peaks

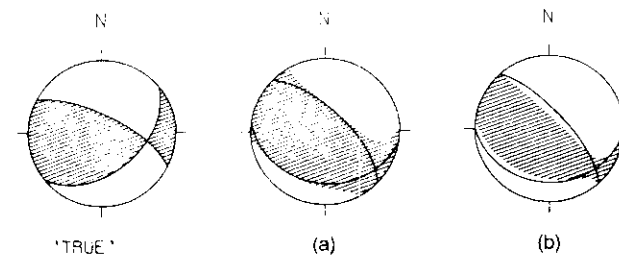

Figure 4. Lower hemisphere equal area projections of the mechanisms obtained from the first peaks of the $M_{ij}(t)$ functions shown in Figs 3(a) and (b), solid lines. The hatched area indicates compressions. Nodal lines correspond to the double couple part obtained by decomposition of the general moment tensor solution. 'True' denotes the focal mechanism of the source used for 'real' record generation (Fig. 2, solid lines).

correspond to a mechanism equal to that shown in Fig. 4(a). The comparison between the $M_{ij}(t)$ functions obtained from the inversion with the 0.5 km discretization step and those obtained from the inversion with the 0.25 km discretization step, shows that the late part of the signal in Fig. 3(a) for $0.15\text{ s} < t < 0.4\text{ s}$ is due to the improper depth location, caused by the too rough discretization step, while the later part of the $M_{ij}(t)$ functions ($t > 0.4$ s) is not reliable in both tests.

Smooth data (Fig. 2b) inverted by using the base functions computed with a depth spacing of 0.25 km give the moment tensor with a shape similar to that shown in Fig. 3(b). A mechanism similar to the previous cases is retrieved (only the volumetric component is greater), the time duration corresponds well to the true one, and the amplitudes following the main pulse are very small.

The non-zero amplitudes of the functions $M_{ij}(t)$ for $t > 0.15$ s, and $t > 0.7$ s, respectively for instantaneous and finite duration sources appear only in the functions $M_{ii}(t)$ ($i = 1, 2, 3$), representing the time dependence of the diagonal elements of the moment tensor. Moreover, these

components of the functions are highly correlated and have comparable amplitudes there, i.e. they represents an apparent additional volumetric component of the mechanism. Thus a simple way to suppress it is to subtract, at each time t, the average $[M_{11}(t) + M_{22}(t) + M_{33}(t)]/3$ from all the diagonal traces $M_{ii}(t)$. The functions obtained after the subtraction (in the following called reduced functions) $m_{ij}(t)$ are plotted in Figs 3(a) and (b) as dashed lines. Most of the spurious signals are removed by this procedure and the source mechanism can be retrieved more satisfactorily than in the case in which the $M_{ij}(t)$ functions are used (in this example the source mechanism is nearly the same as the one shown in Figs 4a and b). When the volumetric part is removed from the $M_{ij}(t)$ functions obtained from the inversion with the 0.25 km discretization step, the reduced $m_{ij}(t)$ functions reproduce very closely the true source duration, and are smoother than the $m_{ij}(t)$ functions computed in the case of 0.5 km depth spacing.

The rotation of the nodal lines visible in Figs 4(a) and (b) with respect to those of the true source (Fig. 4, 'true') is caused by the source–station geometry and it is not influenced by the effects investigated here: it is nearly entirely removed by introducing four additional stations located in the axes of the quadrants defined by the four stations initially considered.

To investigate the ability to reconstruct waveforms with an even more complicated shape, 'observed' ground velocities have been considered. The inversion made with the base functions constructed by means of the depth spacing of 0.5 and 0.25 km gives very similar results to those obtained in the previous tests with displacements, therefore they are not illustrated by figures, but simply briefly described. In all the performed tests the value of the parameter Y is 1. When inverting the records with the base functions computed for an instantaneous source, with a depth spacing of 0.5 km, the source depth is evaluated at 0.81 km, whereas using the base functions computed with a spacing of 0.25 km, the source depth is reconstructed at 0.71 km. When the apparent volumetric part is removed the time duration corresponds well to the true one. In any case the source mechanism is satisfactorily reconstructed.

The use of completely independent time histories for each moment tensor component may give rise to physically questionable results, like, for instance, correlation between the $M_{ij}(t)$ traces and reverse motion. The correlation found between the $M_{ij}(t)$ traces suggests to assign a joint time dependence to all the six moment tensor components and to find six scalar multipliers, λ_i, the product of which with the joint time function would approach the reduced $m_{ij}(t)$ functions as close as possible. To reject reverse motion during the rupturing process the additional condition of a non-negative joint time function is imposed. The joint time function reproduces the source time function, i.e. the time duration of the energy release; the λ_i are the amplitudes of the moment tensor, constant for all the rupture process, and provide the 'average' mechanism of the event. The joint time function gives, when multiplied by the λ_i values, the reduced $m_{ij}(t)$ functions. The joint time function (reported in Fig. 3c), is characterized by secondary amplitudes which are much smaller than those which affect the $m_{ij}(t)$ functions. The corresponding 'average' focal mechanism is totally in agreement with that shown in Fig. 4(a).

3.2 Inversion of records corresponding to a structure defined outside of the range of structures *a priori* chosen

In practice, the uncertainty in the structural parameters can lead to the inversion of records corresponding to a velocity and attenuation distribution not belonging to the range of models chosen: in our parametrization this situation is represented by a value of Y outside of the range $[0, 1]$.

A set of 'observed' records has been generated by using a structural model R (see Fig. 1c), which differs from the model W in the values of the quality factor Q (*cf*. Figs 1b and c). Despite this apparently small change in the structure the seismograms differ significantly. Low-frequency waves have slightly different periods, and high-frequency parts, generated by an instantaneous source, have different amplitudes (see Figs 2a and 5a).

The inversion of these records is performed by using the base functions constructed with the same depth spacing used in Section 3.1. As an example we present only the tests with the instantaneous source and the base functions computed with a depth spacing of 0.25 km (Fig. 5a). The data are not reproduced by the synthetic seismograms so well as in Section 3.1, and this is not surprising since the structure used cannot be resolved by the parameter Y, nevertheless the agreement is still very good [see Fig. 5(a) where even most of the high-frequency arrivals coincide well]. The retrieved depth is located at 0.94 km and the value of the parameter Y is 1, i.e. the structure nearest to the true one has been selected. The good fit between 'observed' and synthetic records constructed for an improper structural model is paid by complexities in the source time function that do not reflect real source characteristics. These functions, obtained by inverting the high-frequency records shown in Fig. 5(a), are presented in Fig. 5(b). It can be seen that the late parts of the source time function are rather complicated, especially the diagonal terms $M_{ii}(t)$ which present large spurious peaks. Useful information about the source mechansim is contained only in the initial part ($t < 0.15$ s) of the functions $M_{ij}(t)$, whose double-couple component displays a good similarity with the true mechanism (see Fig. 5c). The spurious peaks are not removed by the elimination of the volumetric part from the $M_{ij}(t)$ functions (dashed lines in Fig. 5b).

The situation improves when inverting smooth records: the retrieved depth is 0.71 km and the nearest structure to the true one is selected ($Y = 1$). The true source information is masked again by a spurious and correlated signal in $M_{ii}(t)$. The mechanism obtained by considering the first well-pronounced lobe, both in the case of an instantaneous source and a 0.6 s duration, is near to the one obtained by using the 'real' data constructed with the structure W. A further improvement can be made if the reduced $m_{ij}(t)$ functions are used. The mechanism obtained from the early part ($t < 0.7$ s) of the $m_{ij}(t)$ functions is shown in Fig. 5(d). Also in this case the joint time function shows smaller secondary amplitudes than the reduced $m_{ij}(t)$ functions, both when data generated by an instantaneous source or by a time extended source are used. The λ_i values give the same mechanism shown in Figs 5(c) and (d).

The effects due to the use of records computed for a structure not contained in the interpolation range of the base functions are mainly expressed by the apparent

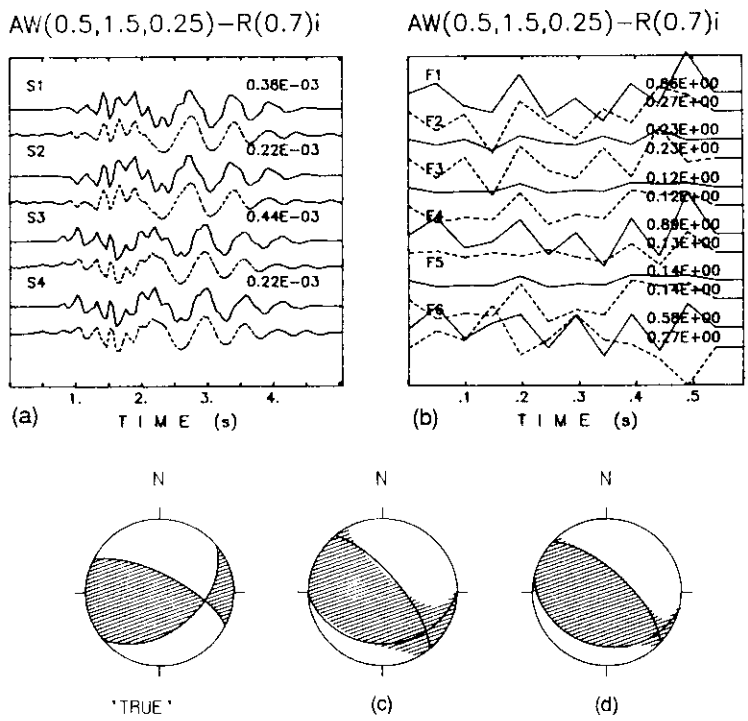

Figure 5. (a) Seismograms generated in the structural model R (solid lines) with the same source parameters as Fig. 2(a). The spacing of the depth grid for base functions computation is 0.25 km. The synthetic seismograms are drawn as dashed lines. (b) Time functions $M_{ij}(t)$ (solid lines) and reduced $m_{ij}(t)$ (dashed lines). (c) Mechanism obtained from the unconstrained $M_{ij}(t)$ functions for $t < 0.15$ s. (d) Mechanism obtained from the inversion using the values of the moment tensor components from the $m_{ij}(t)$ functions for $t < 0.15$ s.

volumetric component of the source. The inversion can therefore be performed with the constraint $M_{11}(t) + M_{22}(t) + M_{33}(t) = 0$, i.e. for a purely deviatoric moment $[M_{ij}(t) = m_{ij}(t)]$. Obviously the agreement of the synthetic seismograms with the data is worse than before, but it is still acceptable (see Fig. 6a and Fig. 5a). The retrieved depth is located at 0.98 km and the value of the parameter Y is 0.65. The corresponding $M_{ij}(t)$ functions are presented in Fig. 6(b). Also in this case, in the joint time function some secondary amplitudes, visible in Fig. 6(b), are eliminated. The retrieved focal mechanism is near to that shown in Fig. 5(d), both when using the first peak of the $M_{ij}(t)$ functions or the λ_i values.

3.3 Test with noisy data

To study the influence of random noise, the 'observed' records are contaminated with noise of amplitude reaching 10 to 25 per cent of the peak signal amplitude. For both noise levels the inversion is performed for 'observed'

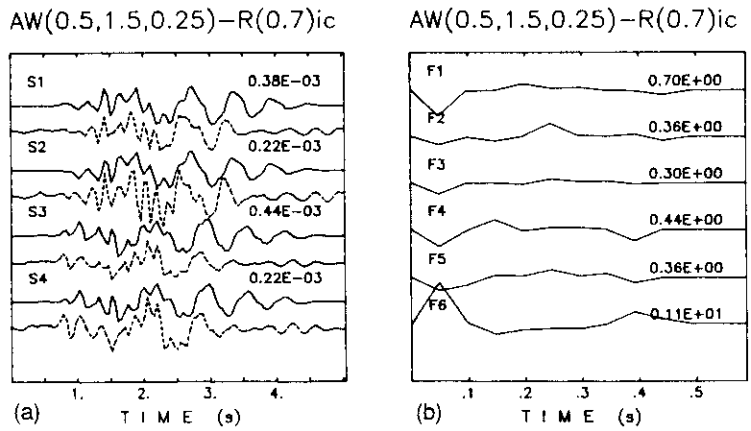

Figure 6. (a) Seismograms generated in the structural model R (solid lines) with the same source parameters as Fig. 2(a) and synthetic seismograms (dashed lines) satisfying the condition of a non-volumetric source. The spacing of the depth grid for base function computation is 0.25 km. (b) $M_{ij}(t)$ functions corresponding to the synthetic seismograms.

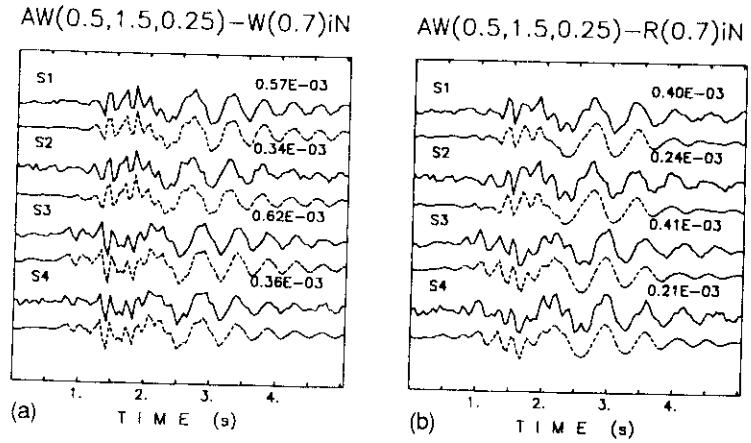

Figure 7. Noisy 'data' (solid lines) corresponding to the instantaneous source with the source parameters given in Fig. 2. The spacing of the depth grid for base function computation is 0.25 km. The noise superimposed on the records is random, with the maximum amplitude reaching 10 per cent of the signal peak amplitude. (a) 'Real' data constructed with the structure W and synthetic seismograms (dashed lines) obtained in the unconstrained inversion which allows a volumetric part in the moment tensor. (b) 'Real' data constructed with the structure R and synthetic seismograms (dashed lines) obtained in the unconstrained inversion.

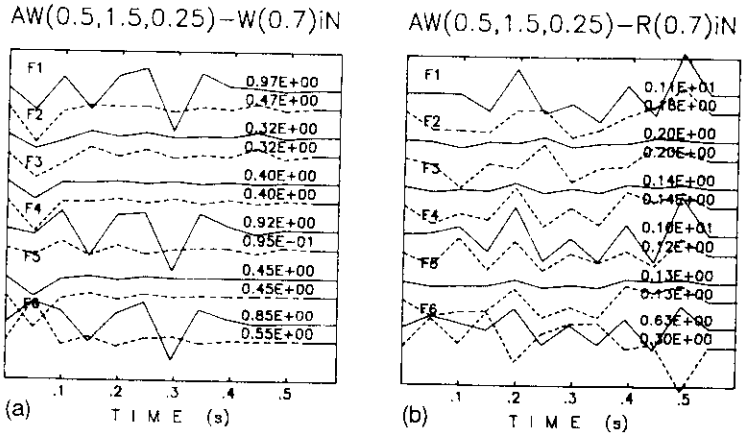

Figure 8. $M_{ij}(t)$ functions obtained by unconstrained inversion of the noisy records shown in Fig. 7 (solid lines), and the reduced $m_{ij}(t)$ functions (dashed lines); (a) refers to Fig. 7(a) and (b) refers to Fig. 7(b).

records generated by both instantaneous and finite-duration sources acting in both W and R structural models. The fit of synthetic seismograms to noisy data is quite nice for all experiments performed [for brevity the data and synthetic seismograms are presented only for a noise level of 10 per cent and an instantaneous source (see Figs 7a and b)].

Inversion of 10 per cent noisy data pertinent to the structure W (Fig. 7a) yields a focal depth of 0.71 km for both instantaneous and finite duration sources. The retrieved value of the structure interpolation parameter is $Y = 0.99$, i.e. the proper structure W is taken for the construction of the final synthetic seismograms. The resulting time functions are presented in Fig. 8(a). The correlated spurious signal introduced by the presence of noise in the records is clearly visible also in the late parts of the functions $M_{ij}(t)$ and useful information can be found in the initial part only ($t < 0.15$ s for high-frequency records, $t < 0.7$ s for smooth records). The mechanism corresponding to $t < 0.15$ s is plotted in Fig. 9(a). The double couple component shows a nice similarity with the solutions

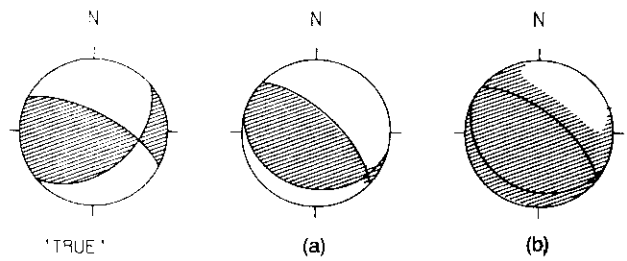

Figure 9. Mechanisms obtained from the first peaks of the time functions $M_{ij}(t)$ (solid lines) shown in Figs 8(a) and (b). For an explanation see the caption of Fig. 4.

obtained without noise (see Fig. 9a and Fig. 4a), while the volumetric and CLVD parts are different from zero, i.e. are not determined correctly. Once the volumetric part is removed, the $m_{ij}(t)$ functions reproduce the source duration well.

When treating 10 per cent noisy records constructed using

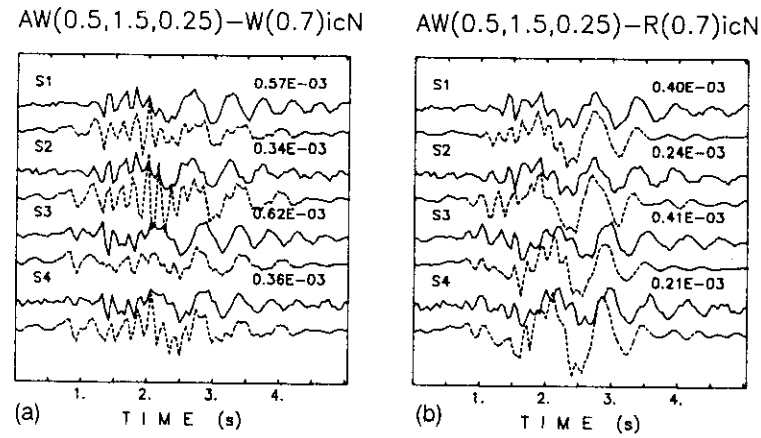

Figure 10. Noisy 'data' (solid lines) generated in structures W and R (for details see caption of Fig. 7). (a) 'Real' data constructed with the structure W and synthetic seismograms (dashed lines) obtained in the constrained inversion (which inhibits the volumetric part of the moment tensor). (b) 'Real' data constructed with the structure R and synthetic seismograms (dashed lines) obtained in the constrained inversion.

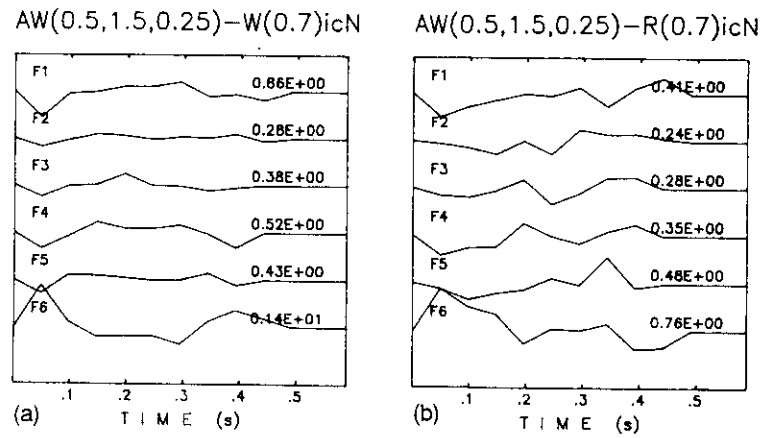

Figure 11. Time functions $M_{ij}(t)$ obtained by the inversion of the noisy records shown in (a) Fig. 10(a) and (b) Fig. 10(b) (solid lines) respectively.

the structure R (i.e. the structure not contained in the range of the parameter Y), the resolution is much worse than in the previous case. For the records generated by an instantaneous source (Fig. 7b), the depth is determined to be equal to 0.94 km and the nearest model (the model W) to the R structure is selected. The inversion of the records corresponding to a finite-duration source gives a depth of 0.73 km very close to the true depth, and the final value of $Y = 1$ corresponds to the model W. Also in this case only the very beginning of the time functions $M_{ij}(t)$ may be used to extract useful information about the source. The mechanisms obtained from the initial part of the time functions display a spurious volumetric component of explosive type; however, as in the previous case, the DC part is nearly the same as that obtained by the inversion of signals without noise. In Fig. 9(b) the mechanism corresponding to the inversion of the data generated by the instantaneous source is presented. As in the case described in Section 3.2, the reduced $m_{ij}(t)$ functions are affected by secondary spurious amplitudes.

Inversion of 10 per cent noisy data performed with the constraint of a non-volumetric source $[M_{ij}(t) = m_{ij}(t)]$ provides synthetic seismograms with a correlation to the data which is worse than that obtained in the unconstrained case (see Figs 10a, b 7a, b) but the main phases are modelled satisfactorily. The $M_{ij}(t)$ functions are reasonable: the pulse corresponding to the proper source time function can be clearly identified for both instantaneous (Figs 11a and b) and time-extended sources acting in the W and R structural models. For the high-frequency records computed by means of the structure R, the reconstruction of the source pulse is better than in the unconstrained inversion and the late spurious large peak has the amplitude significantly reduced (see Fig. 11b and Fig. 8b). The joint time functions, computed in all the tests which have been performed, give source time functions with secondary amplitudes smaller than those present in the corresponding $m_{ij}(t)$ functions and the retrieved mechanisms are completely in accord with those obtained by using the first peaks of the functions.

If the noise reaches 25 per cent of the peak amplitude, the waveform reconstruction is again nice, while the reconstruction of the source time function is difficult. Nevertheless, except for the inversion of the high-frequency records computed for the structure R, such a reconstruction can be done and it provides mechanisms close to those in Figs 9(a)

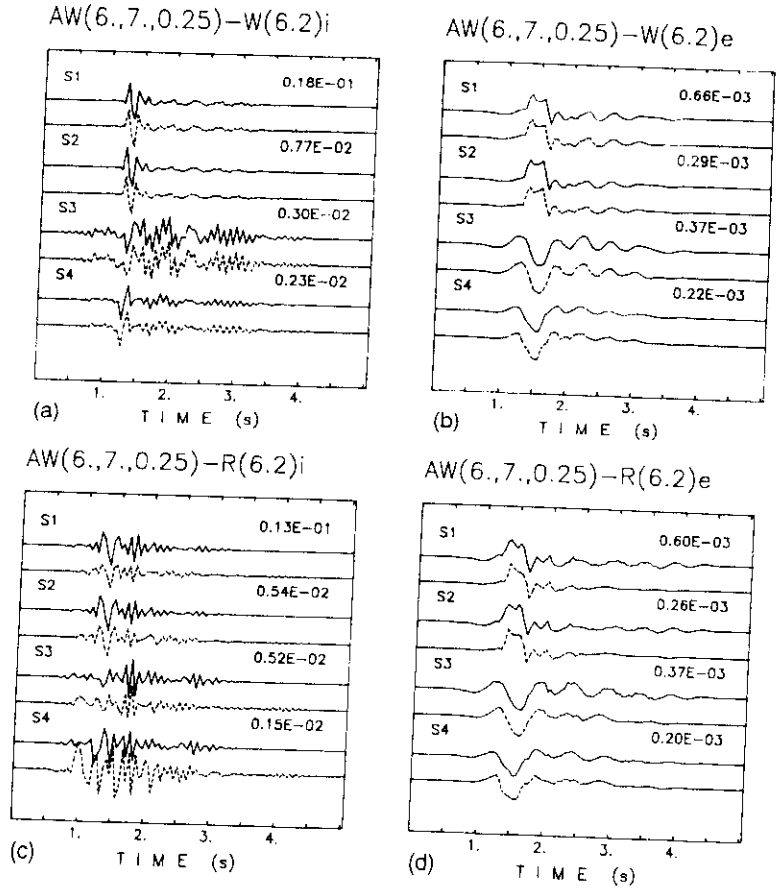

Figure 12. 'Data' (solid lines) and synthetic seismograms (dashed lines) obtained from the inversion with base function interpolation between structures A and W and with 0.25 km grid spacing for depth discretization. The 'data' are generated by an instantaneous point source (a, c) and a source with a duration of 0.6 s (b, d) acting in the structural models W (a, b) and R (c, d). Source parameters: depth 6.2 km, dip 45°, strike 50°, rake 30°.

and (b), even if the proper shape of the source time function cannot be retrieved.

3.4 Inversion for a deeper source

For a source at a depth of 6.2 km we show the results of the inversion of the ground velocities (Figs 12a–d, solid lines). The final synthetic seismograms are very close to the records for all four cases investigated (Figs 12a–d, dashed lines). The inversion of high-frequency records constructed with the model W (Fig. 12a) yields a depth of 6.0 km and a value of Y equal to 1. The $M_{ii}(t)$ functions are highly correlated (Fig. 13a, solid lines), but the large initial peak of the reduced $m_{ij}(t)$ functions corresponds to the true source time function and provides a mechanism sufficiently close to the 'true' one (Fig. 14a). The same mechanism is obtained from the λ_i values associated with the joint time function. When inverting the high-frequency records constructed with the model R the retrieved depth is 6.5 km and the value of Y is 0.45. The $M_{ii}(t)$ functions (Fig. 13c, solid lines) are contaminated by a spurious correlated signal due to the use of a structure outside the range considered. When subtracting the volumetric part of the moment tensor (Fig. 13c, dashed lines), the reduced $m_{ij}(t)$ functions show a dominant peak centred around 0.45 s, which is not consistent with the real source characteristics. If this spurious peak is neglected and we consider the early parts of the $m_{ij}(t)$ functions ($t < 0.15$ s), the mechanism obtained poorly reproduces the 'true' one (only the thrust component is preserved). The use of the joint time function reduces in part the secondary amplitudes, and the mechanism obtained is near to that obtained from the first peak of the $m_{ij}(t)$ functions. The inversion of smooth records generated by means of structures W and R (see Figs 12b and d) gives the hypocentral depth equal to 6.6 and 6.8 km respectively, while the retrieved structural parameters are $Y = 1$ and 0.45 respectively. The diagonal $M_{ij}(t)$ functions present a correlation which in part overrides the true source information (Fig. 13b, solid lines) and, in the case of the structure R, present a high spurious signal centred around $t = 1$ s (see Fig. 13d, solid lines). However, when the volumetric part is removed the pulse corresponding to the true source time function is retrieved both in duration and shape (Figs 13b and d, dashed lines). The corresponding mechanisms are similar to the 'true' one. The reconstructed joint time functions further reduce the secondary spurious amplitudes and the λ_i multipliers give the same mechansims obtained from the first peak of the $m_{ij}(t)$ functions.

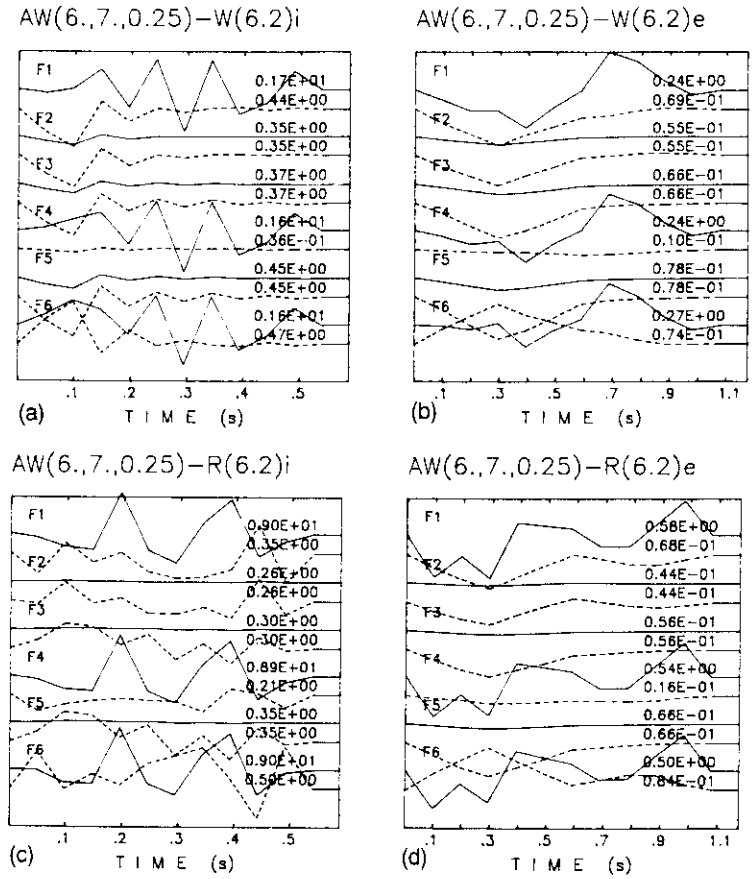

Figure 13. Time functions $M_{ij}(t)$ (solid lines) obtained by the unconstrained inversion of the records shown in Figs 12(a)–(d), and reduced values $m_{ij}(t)$ (dashed lines). (a) $M_{ij}(t)$ and $m_{ij}(t)$ corresponding to 'data' shown in Fig. 12(a). (b) $M_{ij}(t)$ and $m_{ij}(t)$ corresponding to 'data' shown in Fig. 12(b). (c) $M_{ij}(t)$ and $m_{ij}(t)$ corresponding to the 'data' shown in Fig. 12(c), (d) $M_{ij}(t)$ and $m_{ij}(t)$ corresponding to the 'data' shown in Fig. 12(d).

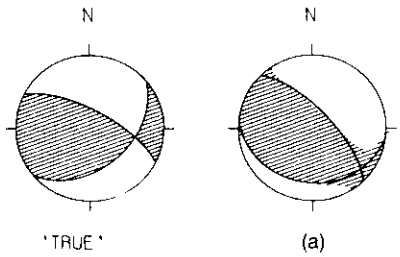

Figure 14. Mechanism obtained using the main peak of the $m_{ij}(t)$ functions shown in Fig. 13(a) as dashed lines. 'True' denotes the focal mechanism of the source used for 'real' records generation (Fig. 12, solid lines).

The results obtained show that, when using high-frequency records, the mechanism and the source time function are satisfactorily reconstructed if the real structure is within the range of structures *a priori* chosen. Therefore, when dealing with real data, if the structural specifications are not known, some caution is necessary in the interpretation of the meaning of the later part of the source time function, which can be satisfactorily retrieved, in its entirety, only when the structural parameters are known with sufficently high detail. When using low-frequency data, the reconstruction of the geometrical and temporal part of the source can also be satisfactory if the real structure is outside of the chosen range.

4 INVERSION OF OBSERVED WAVEFORMS

The method presented in Sections 2 and 3 has been applied to the inversion of five vertical short-period seismograms, proportional to the ground velocity, recorded in the Friuli area (Italy), during the earthquake of 1987 December 27.

The data have been resampled to the same time interval used to compute the base functions (0.0488 s), and successively low-pass filtered to 10 Hz. The station coordinates are given in Table 1. For the hypocentral location we have the three independent estimates listed in Table 1 and corresponding to the 1-D structural models FRIUL7A (model A) (Panza & Suhadolc 1987), FRIUL7W (model W) (Mao & Suhadolc 1992) and OGS (Osservatorio Geofisico Sperimentale 1987). The latitude and longitude values obtained using the OGS model differ by about 0.4 and 0.2 km from those of model A, and by about 0.5 and 1 km from those of the model W. For the source depth, the difference between the values obtained using model

Table 1. Coordinate of the recording stations and hypocentral locations for the event of 1987 December 27.

	Latitude	Longitude
Monte Prat (MPRV)	46°14.5′N	12°59.3′E
Bordano (BOOV)	46°19.2′N	13°06.0′E
Montereale (RCLV)	46°09.6′N	12°39.2′E
Bernadia (BADV)	46°14.2′N	13°14.6′E
Zoufplan (ZOUV)	46°33.4′N	12°58.4′E

Origin time	Latitude	Longitude	Depth	Model
00:21:01.60	46°18.24′N	12°54.84′E	9.47	OGS
00:21:01.28	46°18.44′N	12°54.59′E	9.64	FRIUL7A
00:21:01.55	46°18.34′N	12°55.35′E	7.13	FRIUL7W

OGS and A is about 0.2 km, while this difference is about 2.4 km when the models OGS and W are used. Since we have chosen as extreme structures the models A and W (Figs 1a and b), a first set of tests has been made by assuming the epicentral distances and the origin time obtained from the model W, while in a second set of tests the epicentral determinations and the origin time obtained from the structural model A have been used. On the basis of the depth estimates shown in Table 1 the depth range for the interpolation of the base functions varies from 6 to 10 km. With the depth spacing of 0.5 km, a set of numerical experiments has been performed both with an unconstrained moment tensor and with the non-volumetric constraint, and then for various durations of the $M_{ij}(t)$ functions.

In the first test the analyzed signals have a length of 5.4 s, obtained by applying to the 10 Hz filtered data a D2 window (Press *et al.* 1986) of the same length in time (Fig. 15a, solid lines); the base functions have been constructed with the epicentral determination and the origin time deduced from the model W. The inversion, performed with the unconstrained moment tensor description and the source time function parametrized by 20 time-delayed triangles with half-width $\Delta\tau = 0.0488$ s, gives the synthetic seismograms shown in Fig. 15(a) as dashed lines. The focal depth is determined to about 8.0 km and the final value of the structure interpolation parameter is $Y = 0.97$, which implies that a structure very near to the W model seems to be the most appropriate 1-D representation of the area under study.

The obtained $M_{ij}(t)$ functions and their deviatoric components $m_{ij}(t)$ are shown in Fig. 15(b) as solid and dashed lines respectively. The volumetric component is practically absent. Introducing the scalar multipliers λ_i, defined in Section 3.1, we can get the joint time function shown in Fig. 15(c). From the time function of Fig. 15(c) the earthquake seems to be characterized by two main episodes of release of energy: the first lasting for about 0.5 s and the second around 0.8–0.9 s. On the basis of the results discussed in Section 3.2, the second energy release can be an

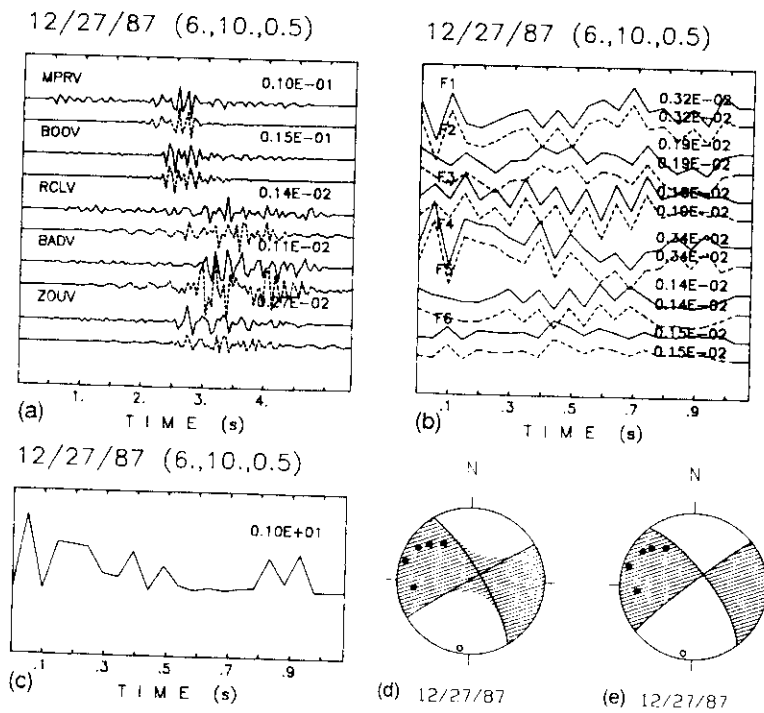

Figure 15. Inversion of waveforms of the Friuli event of 1987 December 27, recorded by five local stations (MPRV, BOOV, RCLV, BADV, ZOUV) at epicentral distances of 8.7, 13.8, 25.9, 26.3 and 28.2 km, and azimuths of 144°, 83°, 232°, 107°, and 8°. Origin time: 00:21:55. (a) Data (solid lines) and synthetic seismograms (dashed lines) obtained with the unconstrained inversion with the base functions constructed in the depth interval 6–10 km with a spacing of 0.5 km; data and synthetic seismograms are truncated with a D2 window with a duration of 5.4 s. (b) $M_{ij}(t)$ functions (solid lines) obtained with the unconstrained inversion and their reduced values $m_{ij}(t)$ (dashed lines). (c) Joint time function, constrained between 0 and 1. (d) 'Average' focal mechanism obtained from the six multipliers λ_i (shaded area: compressions, white area: dilatations) and *P*-wave polarity distribution (open circles: dilatations, full circles: compressions). (e) Focal mechanism obtained from the first significant peak of the $m_{ij}(t)$ functions, shown in (b).

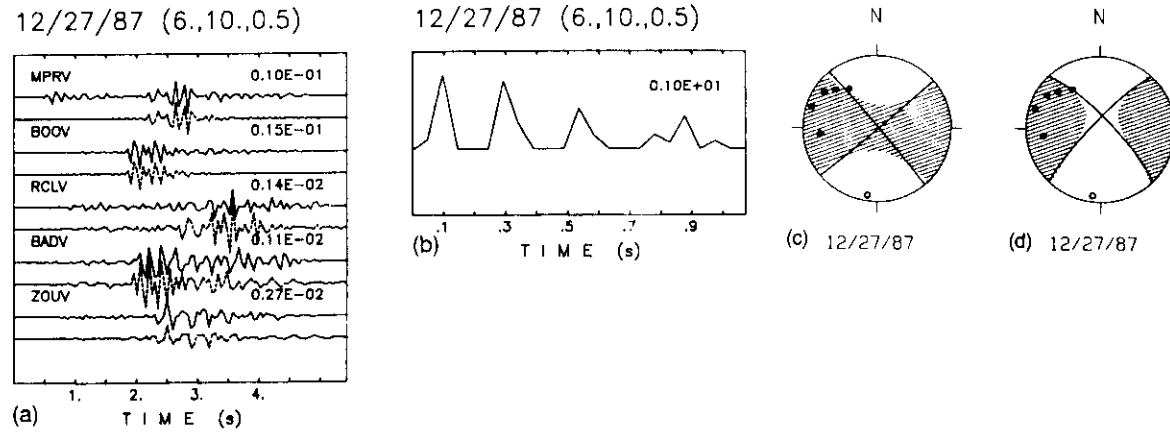

Figure 16. Inversion of waveforms of the Friuli event of 1987 December 27; data (solid lines) and synthetic seismograms (dashed lines) obtained with the unconstrained inversion with the base functions constructed in the depth interval of 6–10 km with a spacing of 0.5 km; epicentral distances of 8.7, 13.8, 25.9, 26.3 and 28.2 km, and azimuths of 140°, 85°, 230°, 107°, and 10°. Origin time: 00:21:28. (a) Data and synthetic seismograms are truncated with a D2 window with a duration of 5.4 s centred in the significant part of each signal. (b) Joint time function relative to the inversion shown in (a). (c) 'Average' mechanism obtained from the six multipliers λ_i associated with the joint time function of (b). (d) Mechanism obtained from the first peak of the functions $m_{ij}(t)$.

artifact introduced by the use of a not completely adequate structural model, but, as will be shown by the analysis of data low-pass filtered at 5 Hz, it can also bear some real information. The value of the seismic moment M_0, obtained from the average ratio between the maximum amplitude of a real signal and the maximum amplitude of the corresponding synthetic seismogram, is equal to 1.0×10^{20} dyne cm. This value, following the relation between the magnitude M and the seismic moment M_0, $M = 2/3 \log M_0 - 10.7$, given by Hanks & Kanamori (1979), is in good agreement with the magnitude (2.9) of the event. The distribution of the few available first arrival polarities (open and solid circles in Fig. 15d) is consistent with the obtained 'average' mechanism (Fig. 15d, shaded areas). The mechanism corresponding to the first peak of the $m_{ij}(t)$ functions is shown in Fig. 15(d) and it is very similar to the 'average' one.

The test performed by using the epicentral distances and the origin time obtained from the model A gives results in agreement with the previous ones (Figs 16a–d). The value of the structural parameter Y is 0.89, i.e. a structure near to the model W is also selected in this case. The retrieved depth is about 7.5 km. The joint time function (Fig. 16b) has a duration quite similar to that shown in Fig. 15(c). In this case the first rupturing episode seems to be formed by three distinct energy releases, centred at about 0.1, 0.3 and 0.55 s. The 'average' mechanism and that deduced from the first peak of the $m_{ij}(t)$ functions are very similar and in agreement both with the polarity distributions and with the mechanisms shown in Figs 15(d) and (e). The only difference is limited to an increment of the CLVD component visible in Figs 16(c) and (d), when compared with Figs 15(c) and (d).

On the basis of the results obtained so far, we have decided to peform some stability tests by using only the base functions computed with the origin time and the epicentral distances deduced from the model W. Some of these tests have been performed by enhancing the contribution of the records with lower amplitudes. The waveform reconstruction improves for the enhanced signals, while it becomes poorer for the records with the largest amplitudes. Moreover the 'average' mechanism and that deduced from the first peak of the $m_{ij}(t)$ functions are in disagreement with the polarity distribution. This is not surprising because the amplitudes recorded in the distant stations are 10 times lower than those recorded in the stations which are nearer to the epicentre. When these amplitudes are made comparable to those recorded in the stations near to the epicentre, i.e. they are amplified 10 times, the consequent amplification of the noise contained in the records can strongly contaminate the inversion.

We have also inverted low-pass filtered data to see if and how the rupture process changes when it is seen at lower frequencies. Using data low-pass filtered at 5 Hz the depth is retrieved at about 9.7 km and the value of the structural parameter Y is 0.9, again very near to the structure W (Figs 17a–c). In this case we have fixed $\Delta\tau = 0.0976$ s. In the joint time function (Fig. 17b) two relatively broad peaks are detected at about 0.4 and 0.8 s. The comparison with the joint time function of Figs 15(c) and 16(c) shows that the low-frequency records practically do not contain information about the initial episode centred at about 0.05–0.1 s. In fact this episode is characterized by a duration which is shorter than the minimum period contained in the 5 Hz low-pass filtered data. On the basis of the experience made with the synthetic data, the presence of the broad peak centred at about 0.8 s can indicate that this energy release is not completely an artifact due to the structural inadequacy. In spite of the large difference in the time history, the resulting 'average' mechanism preserves the strike–slip characteristic and is still in agreement with the few available P-wave polarities and with the 'average' focal mechanism obtained from the high-frequency data. The value of the seismic moment M_0 is in this case equal to 1.2×10^{20} dyne cm and is again in good agreement with the magnitude (2.9) of the event.

Further tests have been performed by varying the length of the inverted signals. Stability in the retrieved depth, in

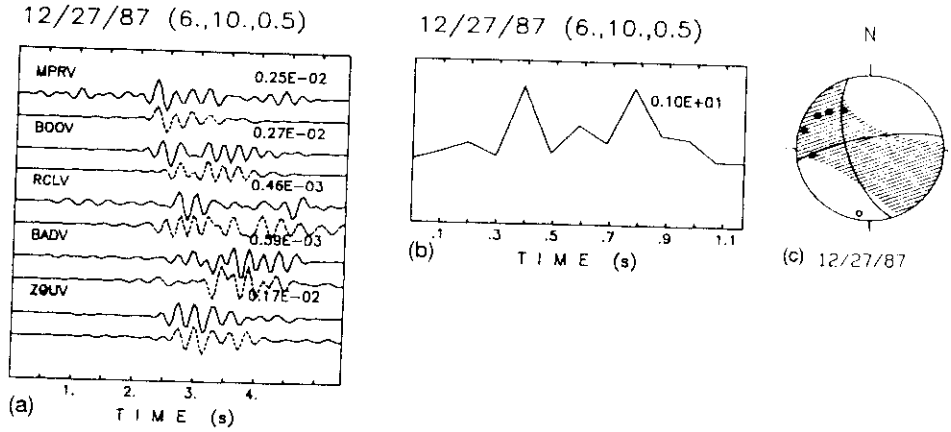

Figure 17. (a) Data (solid lines) and synthetic seismograms (dashed lines) obtained with the unconstrained inversion with the base functions constructed in the depth interval 6–10 km with a spacing of 0.5 km; data and synthetic seismograms are filtered at a cut-off frequency of 5 Hz and truncated with a D2 window with a duration of 5.4 s. (b) Joint time function, constrained between 0 and 1, relative to the inversion shown in (a). (c) 'Average' mechanism obtained from the six multipliers λ_i associated with the joint time function of (b).

the structural parameter and in the plane's orientation deduced from the first peak of the $m_{ij}(t)$ functions, characterized all the tests. The joint time function undergoes some modifications but the character of two distinct energy releases is preserved.

5 Discussion

The knowledge of the proper structural model plays a dominant role in the waveform inversion for the determination of the moment tensor together with its time history. The degree of acceptability of the approximation introduced by the linear interpolation of the base functions depends upon the size of the allowed variability intervals for source depth and structural model: these intervals should be as small as possible.

The synthetic tests demonstrated a good convergence when the structure used to generate the 'observed' records is within the structure interpolation range *a priori* defined. The procedure reconstructs satisfactorily the shape of the 'observed' records and retrieves successfully the source parameters. A slight uncertainty in the focal depth does not seem to affect the correct convergence of the inversion.

Experiments of inversion, performed with the records generated both with instantaneous and time-extended sources show good resolution of all the inverted parameters. The iterative procedure is able to identify the proper structure and the right hypocentral depth. The retrived source mechanism is satisfactorily close to the true one: the moment tensor solution yields, after the decomposition, a dominant double couple component and only a minor share of volumetric and CLVD parts.

The time duration of the source is also retrieved satisfactorily. The moment tensor time functions can, however, be contaminated by spurious signals having their origin in the insufficient precision of the linear base function interpolation, when the depth incremental step is too rough.

The share of spurious correlated signals contained in the moment tensor time functions increases when random noise is superimposed on the records. However rough estimates of the deviatoric component of the source mechanism can be obtained even if the noise reaches about 10 per cent of the peak signal amplitude.

The inversion becomes more problematic when the 'observed' records correspond to a structure outside the range of the structural models *a priori* chosen. The propagation effects, which cannot be accounted for because of the use of an improper structural model, are projected onto the source, and spurious signals appear in the last part of the moment tensor time function. Moreover effects generated by possible rupture spreading in the focal zone are transformed into complexities of the point source time function.

The spurious signals are highly correlated and affect only the traces corresponding to the diagonal elements of the moment tensor. In other words the spurious signals represent the time function of an additional apparent volumetric component of the source. This phenomenon is not surprising because it is the result of matching 'observed' records with the seismograms synthesized by means of improper base functions. These functions are improper in the same way for all the stations used and thus no directivity can appear in the spurious signals representing an isotropic source with a possibly complex time history without any physical meaning. If the structural model differs greatly from the reality, or if very noisy records are considered, the amplitudes of the spurious signals can be large enough to mask entirely the moment tensor time function corresponding to the real source.

There are two ways to remove these spurious signals. The constraint of a non-volumetric source can be imposed on the inversion. This only gives an approximate agreement of the synthetic seismograms with the records, but the moment tensor time functions reflect the source characteristics quite well. However, on the basis of our experience, it seems to be more appropriate to solve the inverse problem for a general moment tensor source and to remove *a posteriori* the volumetric part from the solution of this unconstrained problem.

Following the latter procedure, in most of the synthetic

tests performed, the moment tensor time function and the source duration have been well reconstructed both in duration and in shape.

Taking into consideration all the tests peformed, the application of the technique to experimental data allows us to identify multiple rupture episodes even for a small event ($M = 2.9$). For the earthquake studied the retrieved source mechanism is in agreement with the distribution of the few available *P*-wave polarities.

The systematic application of the technique to several events recorded in the Friuli area as well as the extension of our method to sources of finite dimensions is presently in progress and will be subject of forthcoming papers.

6 CONCLUSIONS

The method of waveform inversion that we have developed allows us to retrieve the moment tensor of a point source as a function of time. In comparison with already existing similar approaches it has the following two advantages.

(1) It allows us to vary the structural model during the inversion; this is accomplished by interpolation between the base functions *a priori* computed for two structural models which can be assumed as acceptable extremes for the region under study.

(2) It allows us to change the focal depth in the course of the inversion, by means of a linear interpolation, with variable spacing, between the base functions *a priori* computed for a set of different depths.

The method provides a good estimate of the complete mechanism when records are treated which correspond to a structural model contained inside the interpolation range, when a sufficiently small incremental step in the focal depth discretization is used and when the contamination by noise does not exceed approximately 10 per cent of the peak signal amplitude. Violation of some of these conditions gives rise to a spurious volumetric component which must be removed. The remaining deviatoric part of the moment tensor contains true information about the source mechanism.

The inversion of the records generated by the Friuli event of 1987 December 27 indicates that also with the case of base functions computed for a 1-D model, it is possible to retrieve satisfactorily the deviatoric part of the mechanism together with the gross feature of its time history. Obviously, a complete retrieval of the source mechanism and its time history will be possible once accurate 3-D models are available together with the proper description of the propagation of complete waveforms in these models.

ACKNOWLEDGMENTS

We are very grateful to ENEA (Computer Center ENEA INFO BOL) for the use of the IBM3090E computer. The research has been performed within the framework of the International Lithosphere Program (ILP)—Theme II-4: Three-dimensional modelling of the Earth's Tectosphere. This study was partly supported by the International Institute for Environmental and Marine Sciences and Technologies (IIEM) of the International Centre for Science and High Technology (ICS) in Trieste, Italy. One of the authors (JS) thanks IIEM authorities for scholarship support. We thank Professor J. Frez for critically reading the manuscript and Dr M. Russi of Osservatorio Geofisico Sperimentale, Trieste, for supplying the experimental data of the Seismological network, supported by the Regione Friuli–Venezia Giulia. We thank the anonymous referees for some very constructive criticisms which helped us in broadening the validity of our method. We also acknowledge financial support from GNDT (CNR contracts nos 89.02015.54 and 90.01007.54), MURST (40 and 60 per cent funds) and PNRA (Linea 5, tema g1–2).

REFERENCES

Aki, K. & Richards, P. G., 1980. *Quantitative Seismology*, Freeman, San Francisco.

CERN, 1985. *Computer Centre Program Manual*, CERN, Geneve.

Frankel, A. & Wennerberg, L., 1989. Rupture process of the M_S6.6 Superstition Hills, California, earthquake determined from strong-motion recordings: application of tomographic source inversion, *Bull. seism. Soc. Am.*, **79**, 515–541.

Gilbert, F.& Dziewonski, A. M., 1975. An application of normal mode theory to the retrieval of structural parameters and source mechanisms from seismic spectra, *Phil. Trans. R. Soc. Lond.*, A, **278**, 187–269.

Hanks, T. C. & Kanamori, H., 1979. A moment–magnitude scale, *J. geophys. Res.*, **84**, 2348–2350.

Hartzell, S. H. & Heaton, T. H., 1983. Inversion of strong ground motion and teleseismic waveform data for the fault rupture history of the 1979 Imperial Valley, California earthquake, *Bull. seism. Soc. Am.*, **73**, 1553–1583.

Jost, M. L. & Herrmann, R. B., 1989. A student's guide and review of moment tensors, *Seism. Res. Lett.*, **60**, 36–57.

Kikuchi, M. & Kanamori, H., 1982. Inversion of complex body waves, *Bull. seism. Soc. Am.*, **72**, 491–506.

Mao, W. J. & Suhadolc, P., 1992. Simultaneous inversion of velocity structures and hypocentral locations: application to the Friuli seismic area NE Italy, *Pageoph*, submitted.

Mendiguren, J., 1977. Inversion of surface wave data in source mechanism studies, *J. geophys. Res.*, **82**, 889–894.

Nabelek, J. L., 1984. Determination of earthquake source parameters from inversion of body waves, *PhD thesis, MIT.*

Ohlson, A. H. & Apsel, R. J., 1982. Finite faults and inverse theory with applications to the 1979 Imperial Valley earthquake, *Bull. seism. Soc. Am.*, **72**, 1969–2001.

Osservatorio Geofisico Sperimentale, 1987. *Bollettino della Rete Sismometrica dell'Italia Nord Orientale*, Trieste.

Panza, G. F., 1985. Synthetic seismograms: the Rayleigh waves modal summation, *J. Geophys.*, **58**, 125–145.

Panza, G. F. & Suhadolc, P., 1987. Complete strong motion synthetics, pp. 135–204, ed. Bolt, A. B., Academic Press, Orlando, FL.

Press, W. H., Flannery, B. P., Teukolsky, S. A. & Vetterling, W. T., 1986. *Numerical Recipes*, Cambridge University Press, Cambridge, UK.

Robinson, E. A., 1967. *Multichannel Time Series Analysis with Digital Computer Programs*, Holden Day, San Francisco.

Šílený, J. & Panza, G. F., 1991. Inversion of seismograms to determine simultaneously the moment tensor components and source time function for a point source buried in a horizontally layered medium, *Studia geoph. geod.*, **35**, 166–183.

Sipkin, S. A., 1982. Estimation of earthquake source parameters by inversion of waveform data: synthetic waveforms, *Phys. Earth planet. Inter.*, **30**, 242–259.

Trehu, A. M., Nabelek, J. L. & Solomon, S. C., 1981. Source characterization of two Reykjanes Ridge earthquakes: surface waves and moment tensors; P wave forms and nonorthogonal nodal planes, *J. geophys. Res.*, **86**, 1701–1724.